12-2015

Rupture in Abdominal Aortic Aneurysm

Qusay Alfaori
University of Arkansas, Fayetteville

Rupture in Abdominal Aortic Aneurysm

A thesis submitted in partial fulfillment
of the requirements for the degree of
Master of Science in Biomedical Engineering

By

Qusay Alfaori
University of Arkansas
Bachelor of Science in Biomedical Engineering, 2014

December 2015
University of Arkansas

This thesis is approved and recommend for the award of degree to the Graduate Council.

_____
Dr. Ashok Saxena
Thesis Director

_____
Dr. Morten Jensen
Ex-officio Thesis Co-Director

_____
Dr. Kartik Balachandran
Committee Member

_____
Dr. Hanna K Jensen
Ex-officio Committee Member

_____
Dr. Woodrow Shew
Committee Member

Abstract

Quantification of abdominal aortic aneurysm development, its growth kinetics, and rupture criteria are important to decrease the risk of this life-threatening event. Uniaxial testing of healthy and collagen degraded aortic specimens from pigs was performed. A mathematical model, from the literature, for the stress-strain relationship that is suitable for describing the behavior of abdominal aortic tissue was used to derive specific tissue properties/parameters as a function of strain rate and as a function of specimen orientation. Analyses consisting of Finite Element Modeling of healthy and collagen degraded abdominal aortas were performed using ABAQUS finite element code and the measured properties. The focus was on finding the values of ultimate tensile strength (σ_{max}), maximum strain at rupture (ε_{max}), elastic modulus (E), and the critical strain (ε_c), identified as the point beyond which high rupture risk is present. These properties vary significantly between healthy tissue and collagen-degraded (aneurysmal) tissue. No significant differences were found in the mechanical properties between longitudinal and circumferential orientation both in healthy and collagen degraded specimens. However, σ_{max}, ε_{max}, and ε_c values were significantly higher for healthy tissue group than for collagen degraded tissue group. For example, $\varepsilon_c = 0.44 \pm 0.08$ versus $\varepsilon_c = 0.0077 \pm 0.0002$ (Mean ± SEM), $\sigma_{max} = 0.93 \pm 0.07$ MPa versus $\sigma_{max} = 0.047 \pm 0.002$ MPa, and $\varepsilon_{max} = 0.87 \pm 0.12$ versus $\varepsilon_{max} = 0.49 \pm 0.10$. In conclusion, the data indicate that collagen is important in maintaining a high critical strain value in healthy abdominal aortic tissue and the risk of AAA rupture increases significantly in the collagen degraded tissue.

Acknowledgement

I would like to express my appreciation and gratefulness to the following people, whose presence, support, guidance, encouragement, and advice were invaluable in this project:

My advisor Professor Ashok Saxena, a “thank you” is not enough to describe how grateful I am for your continuous motivation, encouragement, support, and guidance throughout my research. Your diligence and patience with guiding me through the ups and downs of this research has been much appreciated.

My co-advisor Dr. Morten Jensen, thank you for the patient guidance, enthusiastic encouragement and useful critiques of this research work. Your willingness to give time, knowledge, and effort so generously has been very much appreciated.

Dr. Kartik Balachandran, thank you for your essential help and invaluable advice in this research. I appreciate the knowledge, time, and effort you spent in explaining some of the Biomechanics concepts needed for this work.

Dr. Hanna Jensen, thank you for your creativity, knowledge, and valuable and constructive suggestions during this research work.

Dr. Woodrow Shew, thank you for your knowledge, talent, words of encouragement, and motivation. You have always been so supportive and helpful.

I would also like to extend my thanks to the faculty and staff of the Biomedical Engineering department for their help in offering me the resources needed in this work.

Finally, I wish to thank my parents and friends for their support and encouragement throughout my study.

Dedication

To my father and mother, thank you for all your love and support.
Without you, I would not be where I am today.

Table of Contents

Chapter 1-Introduction: 1
Chapter 2-Literature Review: 8
Chapter 3-Purpose of Study: 41
Chapter 4- Mechanical Testing and Modeling Approach: 43
Chapter 5-Data and Results: 51
Chapter 6-Discussion: 65
Chapter 7-Conclusions: 74
References: 77

List of Tables

Table 1 –. 4
Table 2 – 13
Table 3 – 69
Table 4 – 70

List of Figures

FIGURE 1 –.....3
FIGURE 2 –.....6
FIGURE 3 –.....10
FIGURE 4 –.....11
FIGURE 5 –.....12
FIGURE 6 –.....14
FIGURE 7 –.....15
FIGURE 8 –.....17
FIGURE 9 –.....17
FIGURE 10 –.....18
FIGURE 11 –.....18
FIGURE 12 –.....20
FIGURE 13 –.....21
FIGURE 14–.....21
FIGURE 15–.....22
FIGURE 16 –.....23
FIGURE 17 –.....24
FIGURE 18 –.....24
FIGURE 19 –.....26
FIGURE 20 –.....29
FIGURE 21 –.....30
FIGURE 22 –.....31
FIGURE 23 –.....32
FIGURE 24 –.....32
FIGURE 25 –.....34
FIGURE 26 –.....35
FIGURE 27 –.....36
FIGURE 28 –.....37
FIGURE 29 –.....38
FIGURE 30 –.....39
FIGURE 31 –.....40
FIGURE 32 –.....45
FIGURE 33 –.....47
FIGURE 34 –.....52
FIGURE 35 –.....52
FIGURE 36 –.....53
FIGURE 37 –.....53
FIGURE 38 –.....54
FIGURE 39 –.....55

FIGURE 40 –.....56
FIGURE 41 –.....57
FIGURE 42 –.....58
FIGURE 43 –.....59
FIGURE 44 –.....60
FIGURE 45 –.....60
FIGURE 46 –.....61
FIGURE 47 –.....62
FIGURE 48 –.....63
FIGURE 49 –.....64
FIGURE 50 –.....66
FIGURE 51 –.....67

Chapter 1

Introduction

In spite of the advances in medical sciences, cardiovascular disease remains the leading cause of death in the Western World [1][17]. In the US alone, there are about 81 million people who suffer from at least one form of cardiovascular disease leading to approximately 900,000 deaths annually [1]. In Europe, 40% of deaths among under 75 year old population is from cardiovascular diseases [1, 17]. Abdominal aortic aneurysm (AAA) is an irregular expansion of the abdominal aorta due to the weakening of abdominal aortic wall and is considered as a form of cardiovascular disease.

A patient is said to have AAA when the abdominal aortic diameter is increased by 50% of the healthy original diameter [2]. Every year, 500,000 new patients are diagnosed with AAA throughout the world, 150,000 of those in the United States (?). AAA is present in about 2% of elderly (60 years and older), a population that is rapidly increasing [3][18]. Abdominal aortic aneurysms are the most lethal aneurysms that can develop in the human body, because they have a higher risk of mortality rate approaching 90% upon rupture [1][3]. When AAA rupture occurs, 30-50% patients die before arriving at a hospital, and even after post-surgical treatment, mortality remains at a high rate of 50-70% [1]. Every year in the US, approximately 15000-20000 people die from AAA, and it is listed as the 13th most common cause of death, and the 10th among men that are 55 years of age and older [3].

AAA can be diagnosed using medical imaging techniques such as ultrasonography, computed tomography (CT) scanning, or MRI scanning. Due to technological advancements in medical imaging, AAA diagnosis is increasing worldwide, especially in the west. AAA is often asymptomatic, which makes it difficult for the patients to seek help and to seek treatment. Men who turn 60 years old are prime candidates for AAA screening. However, individuals with family history are at a higher risk of developing AAA at an earlier age. Thus, they are

recommended to be screened for AAA when they turn 50 years old [1]. Figure 1 below shows a healthy abdominal aorta and an aneurysmal aorta.

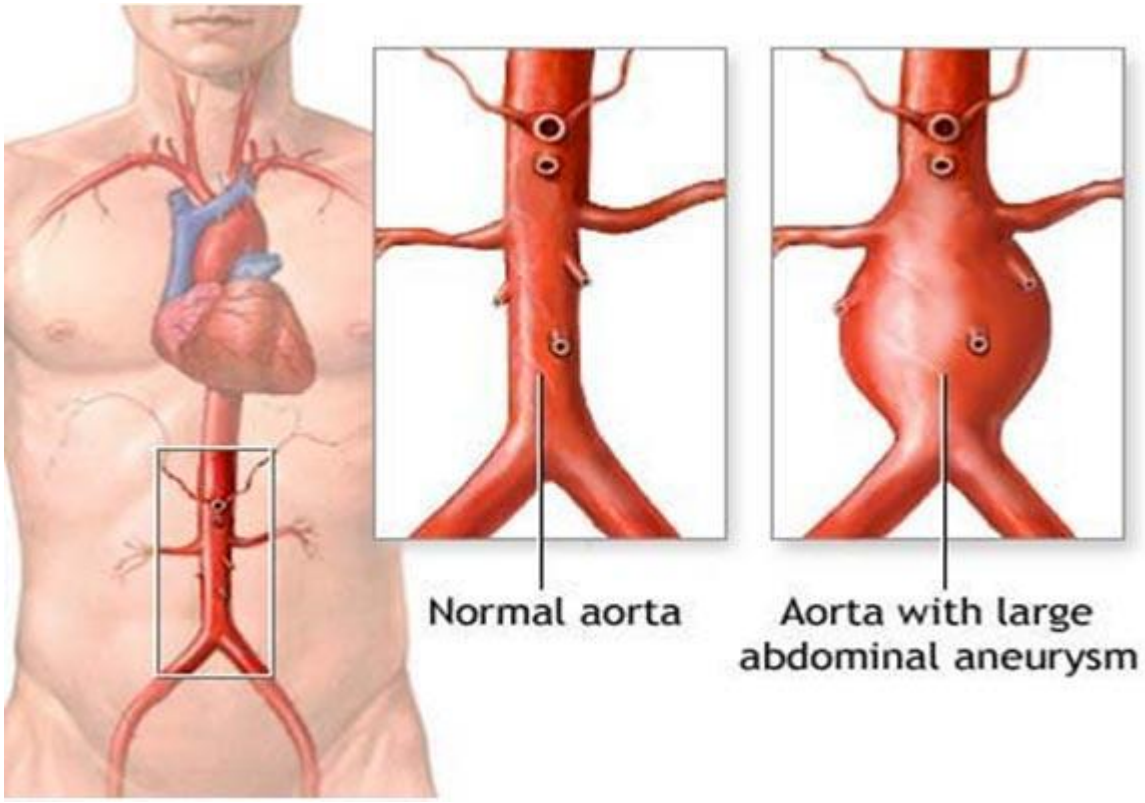

Figure 1 healthy aorta (on the left) and an aneurysmal aorta (on the right) [www.nlm.nih.gov]

Detection of AAA and an assessment of rupture risk of the AAA are both important because the patient's life is potentially at risk. The most common method for rupture risk assessment is measurement of the diameter of the dilated aorta. A healthy aorta measures 2-3 cm in diameter. If the aneurysm exceeds 1.5 times the healthy aorta diameter, then the risk of rupture is considered high at a mortality rate of 95% [3]. Even though some patients have aneurysms that are slightly larger than the normal aorta in diameter, frequent monitoring of such cases is highly recommended in order to assess growth of the aneurysm and to treat it in time to avoid catastrophic rupture.

While not all aneurysms with diameters greater than 1.5 times the healthy diameter rupture, some aneurysms do rupture at diameters less than 1.5 times the original diameter. This observation leads to the conclusion that relying solely on the maximum diameter criteria is not a totally reliable approach to successfully assess the potential risk for rupture. Table 1 shows the percentage of ruptured aortas based on maximum diameter size [3].

Table 1 shows the relationship of size to rupture in 473 nonresected AAA and Percent of ruptured aneurysms for different max diameter sizes of AAA [3].

SIZE (CM)	N RUPTURED	N RUPTURED	TOTAL	% RUPTURED
≤ 5.0	34	231	265	12.8
> 5.0	78	116	194	40.0
NO SIZE RECORDED	6	8	14	43.0
TOTAL	118	355	473	24.9

From the information presented in Table 1, it is shown that aneurysms of various diameter sizes are subject to rupture unexpectedly. Thus, one cannot solely rely on maximum diameter for assessing the rupture risk.

Over the past 15 years, other factors that are considered as relevant to rupture risk assessment are wall stress distribution, wall strength, and formation of intraluminal thrombus (ILT) on AAA wall [1][8][9]. The latter forms due to fluid dynamics-chemical reaction coupled flow. Engineering tools such as finite elements analysis (FEA) are now frequently used to model hypothetical and patient-specific constructed aneurysms. Based on work done using FEA, factors such as expansion rate, degree of symmetry, geometrical parameters of AAA can be used as additional parameters for assessing potential risk of rupture [1].

If the patient undergoes a repair, there are two primary options. The first option is an open surgery, in which the surgeon cuts through the abdomen and places a stent in the aneurysm to bypass the blood flow [4]. This is extremely invasive, costly, and puts the patient at a high risk of infection, and therefore carries with it a high post-surgery mortality rate of 47% (range 27% to 69%) [3]. The second option is endovascular abdominal aortic aneurysm repair (EVAR), where a guided catheter is inserted through the iliac or femoral arteries and is used to guide the stent to the site of the aneurysm. EVAR is not an open surgery, is non-invasive, dramatically reduces the risk of infection, and consequently has a much lower post-surgery mortality rate and therefore highly preferred as an option [4].

The Structure and Anatomy of the Aorta

The aorta is the largest blood vessel (artery) in the body that starts from the left ventricle of the heart and extends to the abdomen, where it branches of to the femoral and iliac arteries, also known as the bifurcation fork. The aorta is divided into four sections as follows: ascending aorta, aortic arch, thoracic aorta, and abdominal aorta. As one descends down the aorta, a gradient of tissue mechanical properties exist that depend on the content of smooth muscle and two main proteins that make up some of the building blocks and the microstructure of the aortic wall. The two main proteins of interest are collagen and elastin. Collagen gives the aortic wall the strength, and elastin gives the ability to recoil [16][19]. Elastin is mainly responsible for the elasticity of the tissue, which is defined as the ability to return to its original shape after being deformed [19].

Any changes in the content of elastin and collagen will result in changing the properties of the aortic wall and may result in smooth muscle degradation. It is composed of three main

layers, from inside to outside, the intima, the media, and the adventitia layers. The anatomy of the aortic wall is shown in Figure 2.

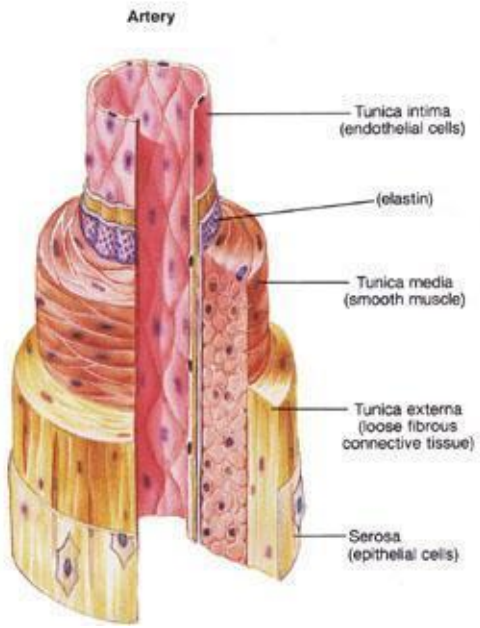

Figure 2 The three main layers of the aortic wall are intima, media, and adventitia (externa and Serosa) [http://www.stiffarteries.com/arterial-stiffness.php].

The development of AAA is not fully understood, but it is known that degradation of the aortic wall causes an aneurysm to form due to changes in wall properties, which in turn causes the aortic wall to become weaker [20]. Wall degradation is a biological process, which can be affected by many factors such as hypertension, atherosclerosis, smoking, chronic obstruction pulmonary disease, gender, age, and family genetic history [3]. Smoking in particular is considered harmful because it directly weakens the walls of the aorta and promotes atherosclerosis [20].

According to Raghaven et al. the stress-strain relationship of aortic tissue is a non-linear exponential curve, where in elastin is continuously involved in supporting the tissue and collagen

fibers start to support the tissue as higher stress is applied [5]. To provide a focus to this study, it is important to address the following two questions: (a) How does collagen degradation contribute to developing AAA and (b) what is the effect of collagen degradation on the tissue's elastic modulus? It is likely that abnormal collagen degradation overtime causes the aortic tissue to develop AAA faster. Thus, quantification of abdominal aortic aneurysm development, growth kinetics, and rupture criteria involving collagen degradation is the main focus of this study.

Chapter 2

Literature Review

Once the aortic wall has degraded sufficiently and is not able to withstand the pressure applied by the luminal blood flow, it is at a high risk for rupture and the patient life is at a very high risk for death. AAA patients are typically asymptomatic; thus, rupture can occur at any time without any warning [6].

There are several predictors of impending AAA rupture: maximum transverse diameter of the aorta, cyclic strain measured via ultra-sound imaging, intraluminal thrombosis (ILT) volume, expansion rate of aortic diameter, and applied wall stress [6]. Some studies have hypothesized that that peak wall stress is a better predictor of rupture than maximum transverse diameter [6].

Peak wall stress can be estimated using computational methods. Finite element method (FEM) is a computational method that is frequently used to calculate peak wall stress in patient-specific cases. Many FEM models have been created so far [6][7][8][9][11]. Each model assumes different aortic properties. Some models assume elastic or viscoelastic tissue behavior, isotropic or anisotropic properties, uniform or non-uniform wall thickness, and with or without considering ILT effects [6].

Geest et al. used FEM to evaluate ruptured and electively repaired AAA [6]. They obtained CT scan images of the AAAs and used them to reconstruct the geometry of the AAA. Their new model included both wall stress and strength distribution. They used the ratio of wall stress to wall strength and introduced a quantity that they termed as rupture potential index (RPI). Consequently, RPI can be used as a qualitative measurement of the potential for rupture. As RPI approaches 1, rupture becomes imminent [6].

Gasser et al. evaluated FEM as a predictor tool for assessment of AAA rupture potential and used A4research diagnostic software to reconstruct and segment the geometry of AAA from

CT scans [7]. They tested four different models of FEM. First, the W model, assumes a constant wall thickness of 2.0 mm and no ILT (intraluminal thrombus). Second, called the PW model, assumes varying wall thickness that changes proportionally with the mean arterial pressure (MAP). MAP = $P_d + (1/3)*(P_s-P_d)$, where P_s and P_d are systolic and diastolic pressures, respectively. Third, called the WT model, assumes both ILT volume and varying wall thickness that ranges between 1.13 to 1.5 mm. Fourth, known as the PWT model, assumes the same conditions as the WT model and on top of that adjusts the wall thickness according to MAP. They concluded that the presence of ILT in the model affects the tissue biomechanics and rupture risk assessment drastically. Also, including ILT and variable wall thickness improves the accuracy of prediction from biomechanical simulations. However, none of the models used could explain rupture in all aneurysmal abdominal aortas for which the data are available [7].

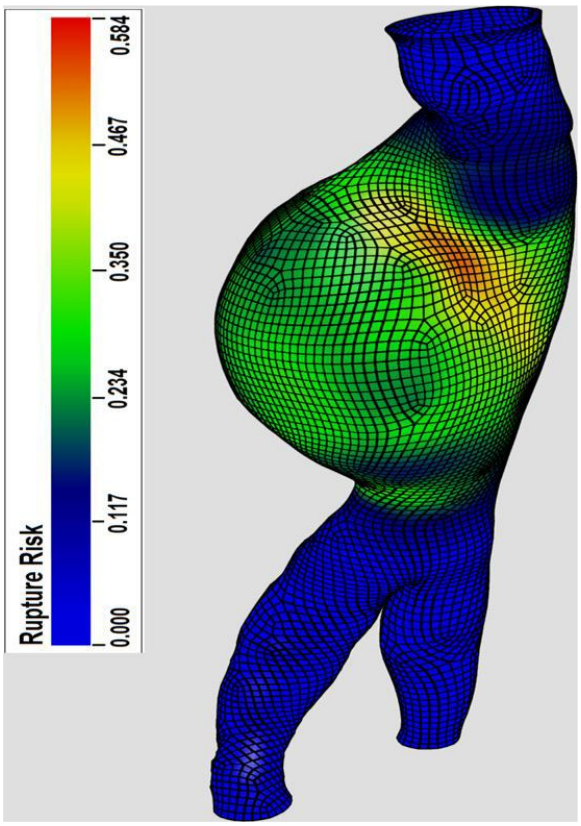

Figure 3 RPI prediction of rupture risk for a patient-specific aneurysm using FEM with 28000 nodes [7].

Biasetti et al. proposed a model to study the fluid-chemical integration in order to observe its role in the formation of ILT in AAA [8]. For the geometry of the AAA, They created a 2D-axis symmetric AAA model to mimic a fusiform aneurysm. The aneurysm is a small fusiform aneurysm of 4.4 cm in luminal diameter, which is clinically, a relevant size to affect blood flow. See figure 4 [8].

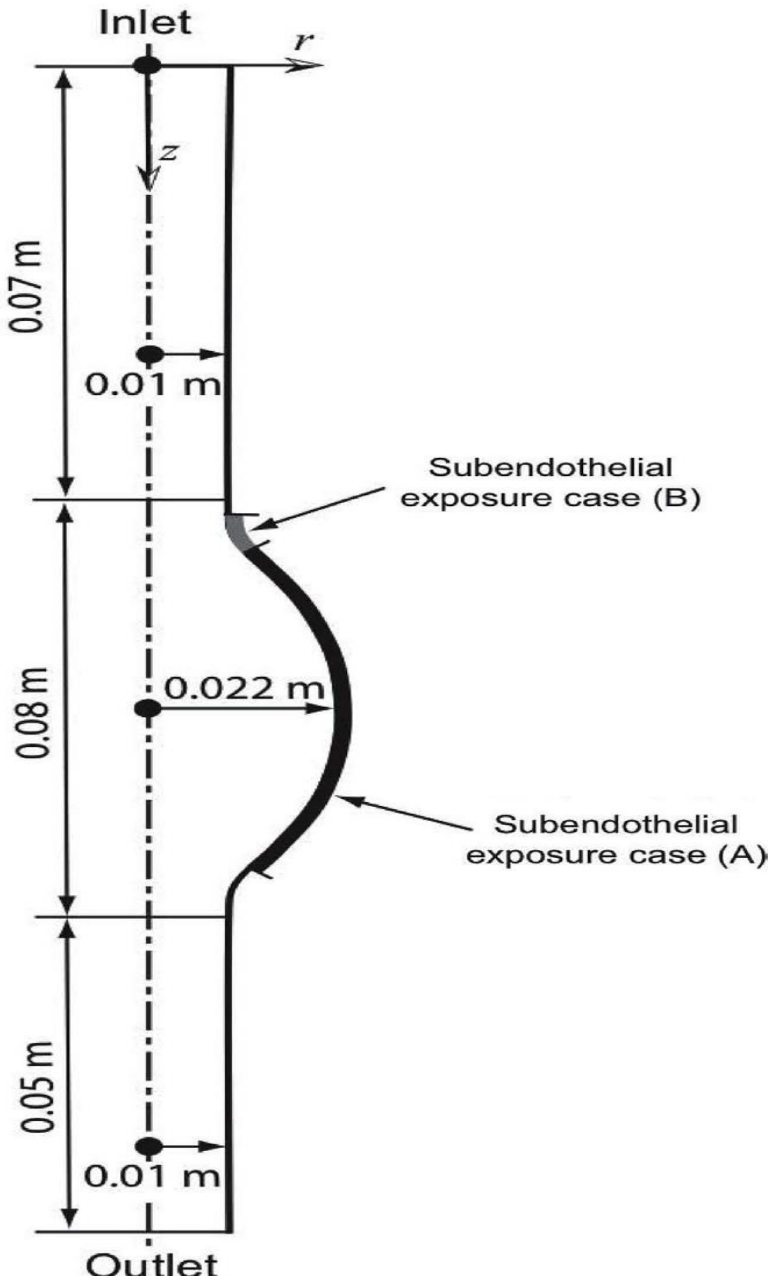

Figure 4 shows an axissymetric fusiform AAA. Case A is a large exposure of subendothelial exposure, and case B is a small exposure of subendothelial exposure [8].

ILT is considered in this model as a thin-layer covering the wall of the aneurysm. Looking at figure 4, case A considers a large exposed area of endothelial cells, where case B considers a relatively much smaller area. The purpose of considering the two cases is to observe the effects of different size of sub-endothelium exposure in ILT formation and, ultimately, blood flow. Figure 5 show the details of the triangular mesh used in the model and concentration and velocity of the boundary layers:

No. of elements	DoF fluid	DoF CDR	Element quality *q*
58,194	268,401	547,254	>0.81

Degrees of freedom is denoted by DoF, and the quality of the triangular elements is given as $q = \frac{4\sqrt{3}A}{h_1^2+h_2^2+h_3^2}$ *(COMSOL, 2008), where A and* h_i, $i = 1, 2, 3$ *denote element area and edge lengths, respectively.*

For the fluid dynamics model, they used the continuity and Navier-Stokes equation.

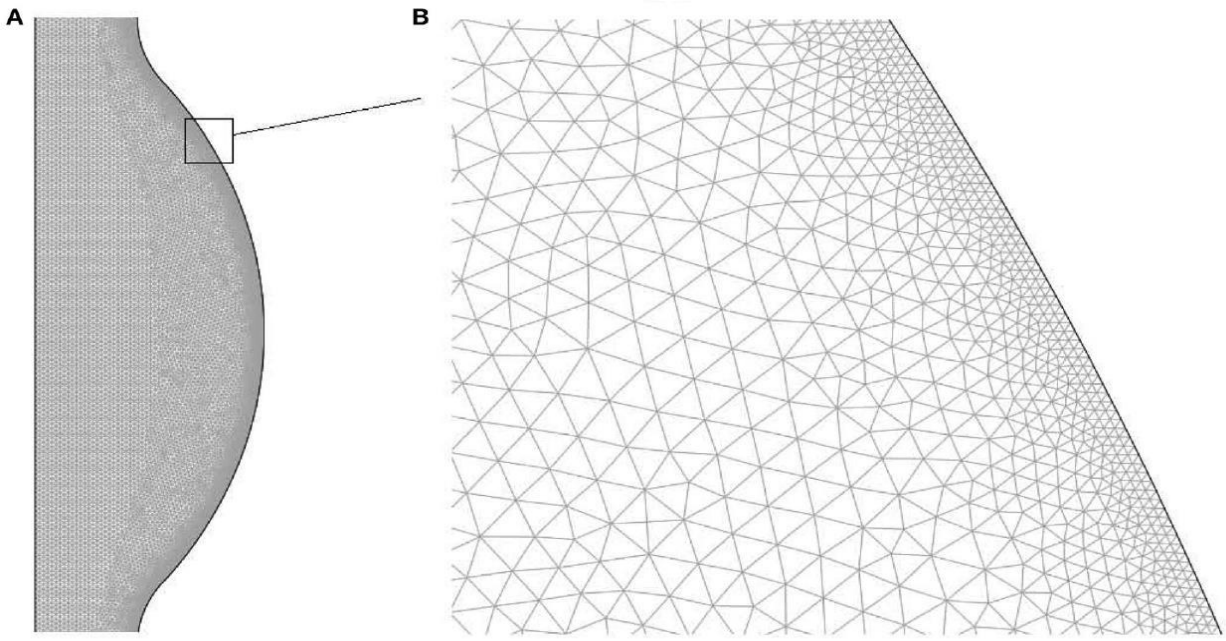

Figure 5 shows the finite element mesh used. Section A, which is the bulge region, and section B, which is a zoom-in of the near wall region [8].

$$\nabla . \boldsymbol{u} = \mathbf{0} \qquad (\mathbf{1})$$

$$\boldsymbol{\rho}\left(\frac{\partial \boldsymbol{u}}{\partial \boldsymbol{t}} + \boldsymbol{u} . \boldsymbol{\nabla u}\right) = -\boldsymbol{\nabla p} + \boldsymbol{\nabla} . \boldsymbol{\tau} \qquad (\mathbf{2})$$

Where **u** is the velocity vector, ρ is density, p is pressure, and $\boldsymbol{\tau} = 2\mu\mathbf{D}$ the deviatoric viscous stress tensor.

To model the fluid, blood in this case, they used the Carreau-Yasuda (CY) blood model as in equation 3.

$$\frac{\boldsymbol{\mu} - \boldsymbol{\mu}_\infty}{\boldsymbol{\mu_0} - \boldsymbol{\mu}_\infty} = [\mathbf{1} + (\boldsymbol{\lambda}\dot{\boldsymbol{\gamma}})^{\boldsymbol{a}}]^{\frac{\boldsymbol{n-1}}{\boldsymbol{a}}} \qquad (\mathbf{3})$$

Where $\boldsymbol{\mu_0}$ *and* $\boldsymbol{\mu}_\infty$ are fluid viscosities, parameters $\lambda, n,$ *and* a define the transition between the lower and upper ends of the shear rate spectrum, $\dot{\boldsymbol{\gamma}} = \sqrt{\mathbf{2}\boldsymbol{D}:\boldsymbol{D}}$ is the scalar shear rate term with $\boldsymbol{D} = (\boldsymbol{l} + \boldsymbol{l}^{\boldsymbol{T}})/\mathbf{2}$ being the symmetric part of the velocity gradient tensor $\boldsymbol{l}$. Also, $\boldsymbol{\Omega} = (\boldsymbol{l} - \boldsymbol{l}^{\boldsymbol{T}})/\mathbf{2}$ which is the antisymmetric part of $\boldsymbol{l}$, was introduced into the model. The CY model describes blood as a Newtonian fluid. The CY parameters used in this model are listed in table 2.

Table 2 CY parameters values

$\boldsymbol{\mu_0}$	$\boldsymbol{\mu}_\infty$	$\boldsymbol{\lambda}$	$\boldsymbol{n}$	$\boldsymbol{a}$	$\boldsymbol{\rho}$
$\mathbf{0.16}\ \boldsymbol{Pa.s}$	*0.0035 Pa.s*	*8.2 s*	*0.2128*	*0.64*	*1050 Kg/m³*

Also, Coagulation cascade that causes thrombin formation was considered in this model. The extravascular tissue factor (TF) is present under the sub-endothelial layer. TF binds to blood-borne factor VIIa upon exposure of sub-endothelial layer to the blood. TF binding with blood-borne factor VIIa initiates the coagulation cascade. The coagulation cascade employs a group of factor enzymes which activate one another, and ultimately aids in the formation of active thrombin as shown in figure 6 [8].

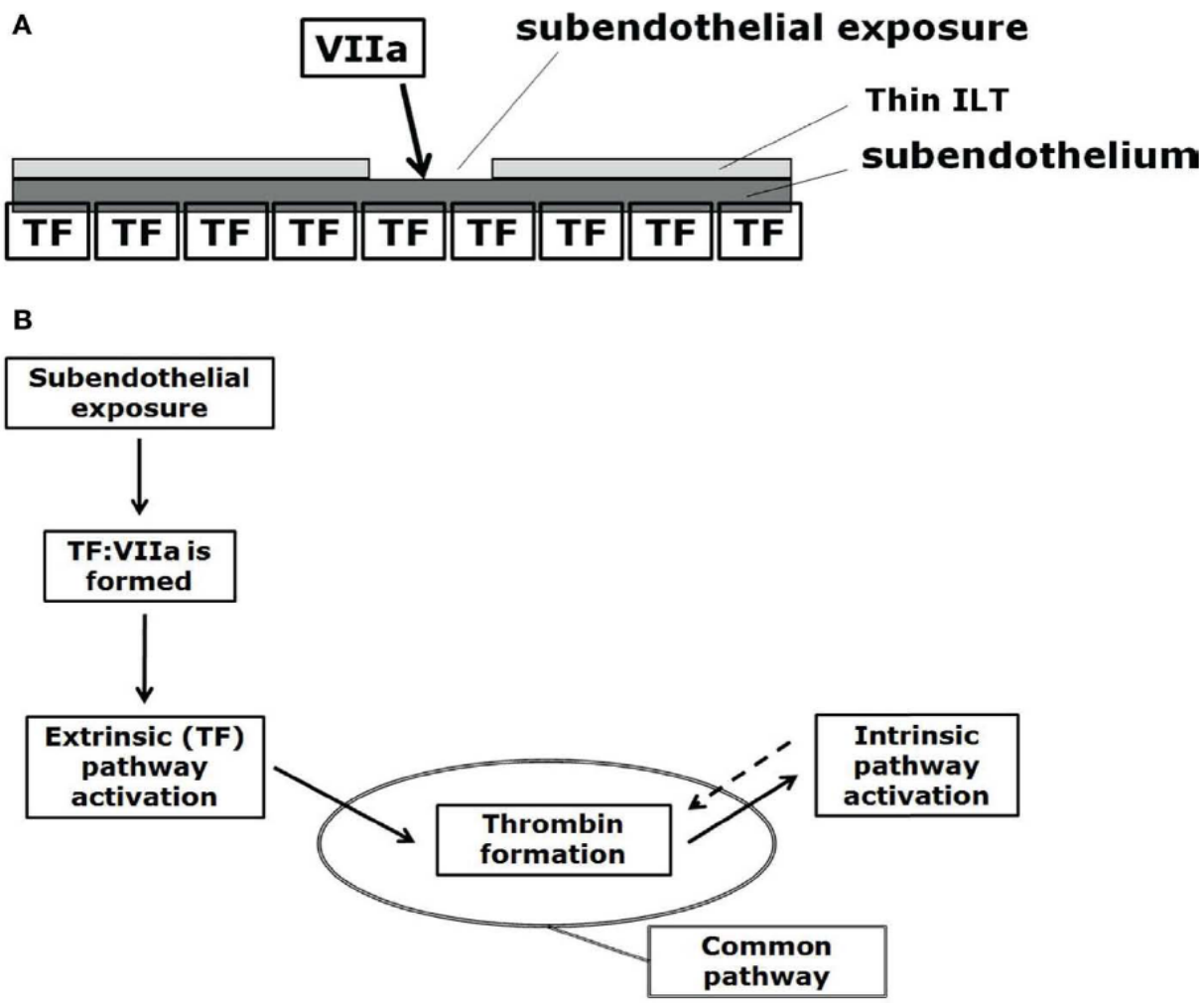

Figure 6 demonstrates A, when the subendothelial layer is exposed and TF binds to blood-borne factor VIIa to initiate the coagulation cascade, and B, where the steps of the coagulation cascade are shown for thrombin formation [8].

Some of the proenzymes and enzymes that are employed in the coagulation cascade were considered in this model [8]. The coagulation cascade is time-dependent; thus, 16 chemical reactions and their associated proenzymes and enzymes are implemented in the model as shown in figure 7. Also, the initial concentrations of the initial enzymes and the rate constants values for the 16 reactions were employed in the study [8].

$$\mathrm{IX} + \mathrm{TF} : \mathrm{VIIa} \underset{k_{16}}{\overset{k_6}{\rightleftharpoons}} \mathrm{IX} : \mathrm{TF} : \mathrm{VIIa} \xrightarrow{k_{11}} \mathrm{TF} : \mathrm{VIIa} + \mathrm{IXa},$$

$$\mathrm{X} + \mathrm{TF} : \mathrm{VIIa} \underset{k_{17}}{\overset{k_6}{\rightleftharpoons}} \mathrm{X} : \mathrm{TF} : \mathrm{VIIa} \xrightarrow{k_{12}} \mathrm{TF} : \mathrm{VIIa} + \mathrm{Xa},$$

$$\mathrm{X} + \mathrm{VIIIa} : \mathrm{IXa} \underset{k_{18}}{\overset{k_6}{\rightleftharpoons}} \mathrm{X} : \mathrm{VIIIa} : \mathrm{IXa} \xrightarrow{k_{13}} \mathrm{VIIIa} : \mathrm{IXa} + \mathrm{Xa},$$

$$\mathrm{IX} + \mathrm{Xa} \xrightarrow{k_{15}} \mathrm{Xa} + \mathrm{IXa},$$

$$\mathrm{V} + \mathrm{Xa} \xrightarrow{k_1} \mathrm{Xa} + \mathrm{Va},$$

$$\mathrm{VIII} + \mathrm{Xa} \xrightarrow{k_3} \mathrm{Xa} + \mathrm{VIIIa},$$

$$\mathrm{V} + \mathrm{IIa} \xrightarrow{k_2} \mathrm{IIa} + \mathrm{Va},$$

$$\mathrm{VIII} + \mathrm{IIa} \xrightarrow{k_4} \mathrm{IIa} + \mathrm{VIIIa},$$

$$\mathrm{II} + \mathrm{Va} : \mathrm{Xa} \underset{k_{19}}{\overset{k_6}{\rightleftharpoons}} \mathrm{II} : \mathrm{Va} : \mathrm{Xa} \xrightarrow{k_{14}} \mathrm{Va} : \mathrm{Xa} + \mathrm{mIIa},$$

$$\mathrm{mIIa} + \mathrm{Va} : \mathrm{Xa} \xrightarrow{k_5} \mathrm{Va} : \mathrm{Xa} + \mathrm{IIa},$$

$$\mathrm{VIIIa} + \mathrm{IXa} \underset{k_9}{\overset{k_7}{\rightleftharpoons}} \mathrm{VIIIa} : \mathrm{IXa},$$

$$\mathrm{Va} + \mathrm{Xa} \underset{k_{10}}{\overset{k_8}{\rightleftharpoons}} \mathrm{Va} : \mathrm{Xa}.$$

Figure 7 shows the reactions cascade incorporated within the model [8].

A concentration vector c (mol/m^3) is introduced in the model due to the reaction rate that takes place due to blood interaction with the endothelial layer of the wall. $\frac{dc}{dt} = \boldsymbol{Sr}$, where **S** is a 18X16 stoichiometric matrix and **r** is a reaction rate vector (mol/m^3s). Also, Convection-Diffusion model is implemented in this model because the chemical reaction is considered as a function of time only and well-mixed, resembling a batch reactor in a sense. To precisely analyze complex flow fields, the concept of coherent vertical structure (VS) is applied to the model, too. The $\lambda_2$method is widely accepted as a method for the analysis. "A vortex is a flow region with predominance of vorticity surrounding a local pressure minimum" [8]. The Navier-Stokes equation is reduced to equation 4 under incompressible flows with no unsteady straining and no viscous effects assumptions:

$$\mathbf{D^2 + \Omega^2 = -\frac{1}{\rho}\nabla(\nabla p)} \qquad (4)$$

This form of the Navier-Stokes equation allows to analyze the pressure minima points in relation to vertical motion; a vortex is a connected region with two negative eigenvalues of $D^2 + \Omega^2$. Because of symmetry, the eigenvalues of $D^2 + \Omega^2$ are real. For eigenvalues $\lambda_1 \geq \lambda_2 \geq \lambda_3$, and $\lambda_2 < 0$, the presence of a VS is indicated. $\lambda_2 = \lambda_{2tr}$ is applied, λ_{2tr} is a defining value of the surface of a VS [8].

Figures 8, 9, 10, and 11 show the results of the coagulation cascade (CC), VS dynamics coupled with flow field, spatially averaged wall shear stress, and thrombin distribution models, respectively:

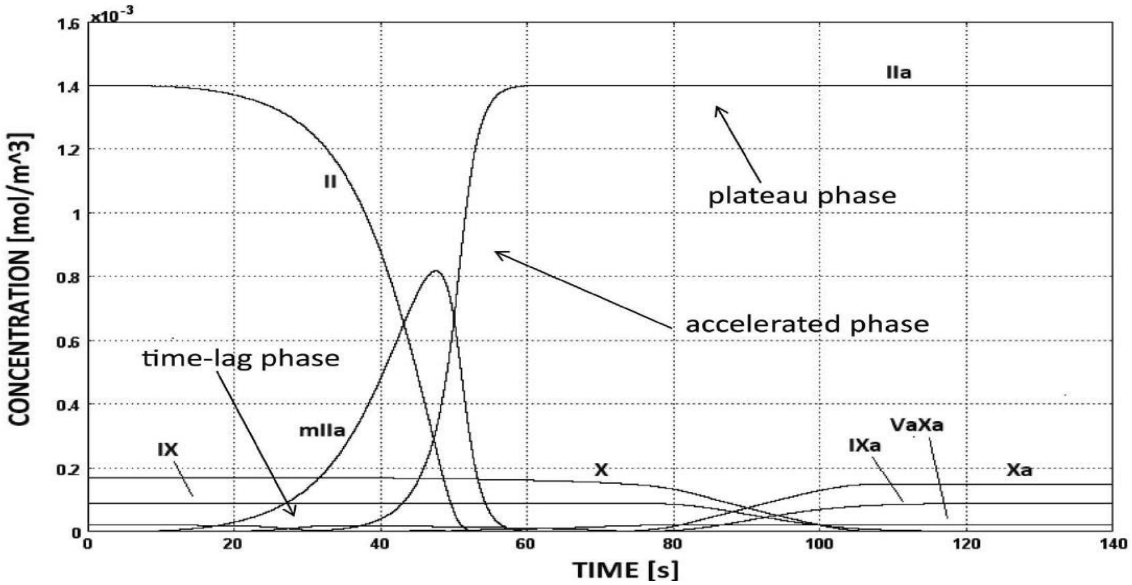

Figure 8 shows the concentration of some the enzymes as blood flows and a chemical reaction takes place with the AAA wall. The three distinct phase of thrombin formation are time-lag, accelerated, and plateau phases, as shown [8].

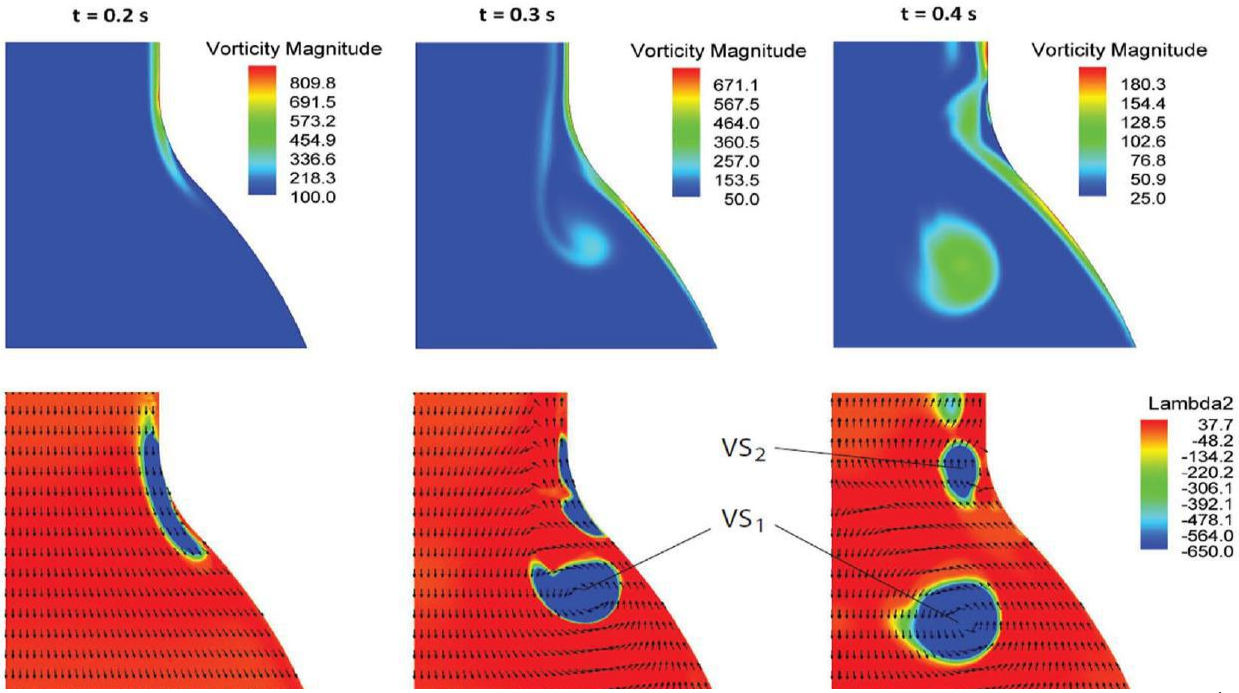

Figure 9 shows, for three different time points of the cardiac cycle, the vorticity magnitude (s^{-1}) in the first row, and VSs values using the Lamda2 method (s^{-2}) in the second row [8].

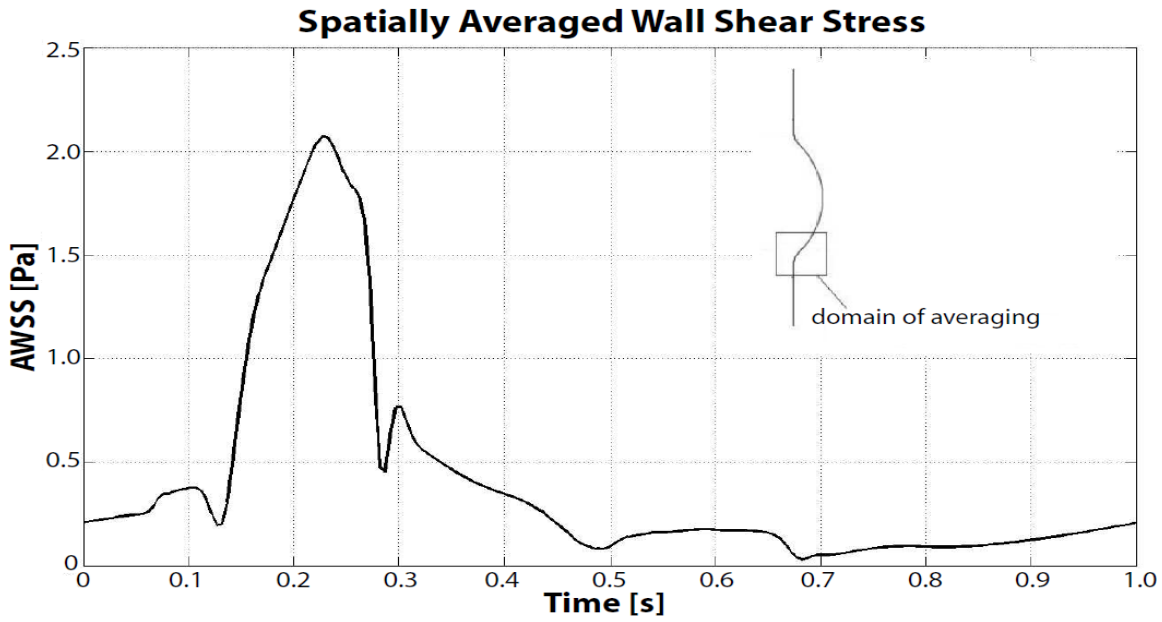

Figure 10 shows the spatially averaged wall shear stress (AWSS) vs time during contraction phase (systolic) of cardiac cycle. It is shown that AWSS increased by about 4 folds during VSs impingement (t=0.15 s to 0.4 s) with respect to relaxation phase (diastolic) of cardiac cycle [8].

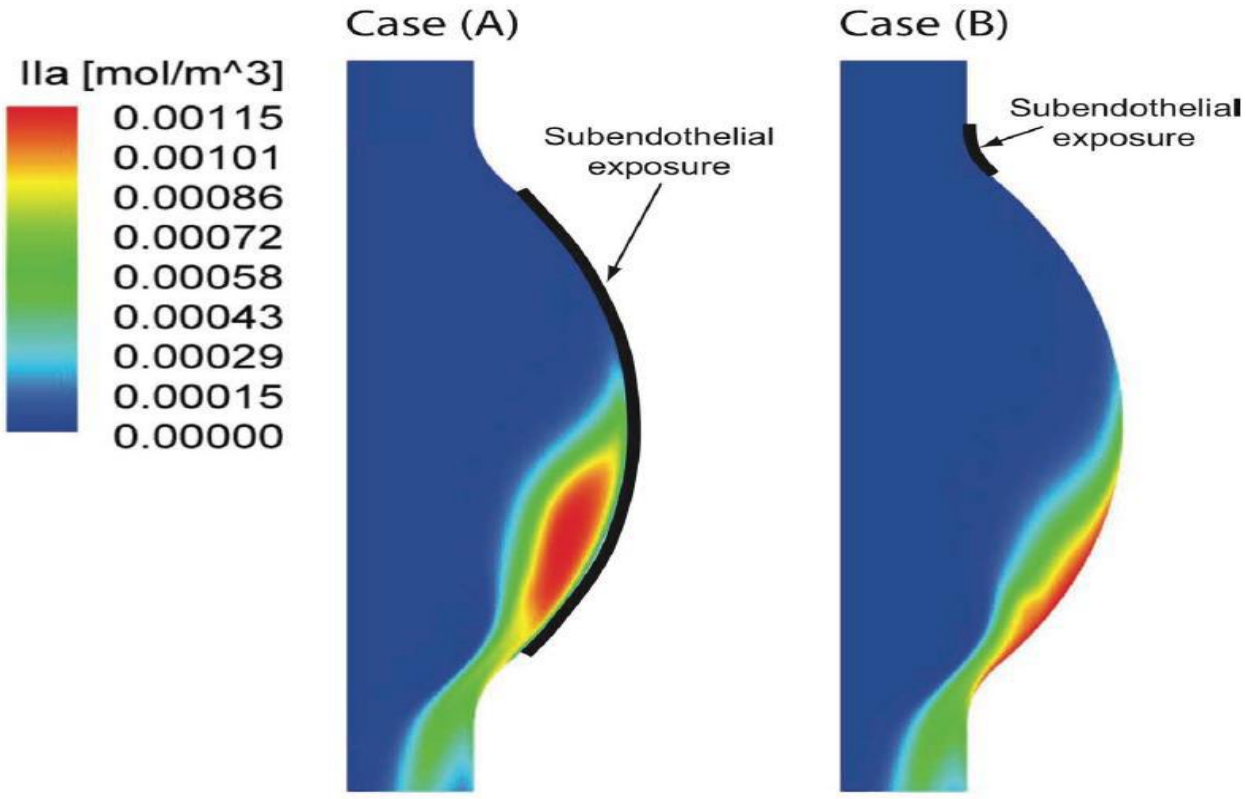

Figure 11 demonstrates thrombin formation for case A, large subendothelial exposure, and case B, small subendothelial exposure [8].

Thrombin formation in the lumen of the aorta is triggered when the interior wall of the aorta is degraded, and the subedothelial layer is exposed to factor IX and X in the blood [8]. The production of thrombin is slow at first, rapidly increases when the intrinsic pathway is activated, and, finally, it reaches a plateau phase, refer to figure 8. It can be concluded that large damaged areas of the AAA will result in large endothelial layer exposure to the flowing blood, affecting blood flow, and ultimately increasing the rate of thrombin formation [8].

The presence of thrombin alters the trajectory of fluid flow in the region of the aneurysm cavity, and it causes complex flow fields to generate, also known as coherent vertical structures VSs [8]. VSs resemble turbulent fluid flow in a way, see figure 9. When intense VSs interact with the layer of the thrombus mass, shear stress spikes as shown in figure 10. An increase in shear wall stress against the thrombus can result in the release of small emboli into the blood stream. Such emboli will circulate in the body and can potentially cause strokes. When more surface area of the subedothelial layer is exposed to the blood, more thrombin formation occurs. The turbulence nature of blood flow in the aneurysmal region causes thrombin to form in the distal part of the aneurysm. For both cases, A and B, shown in figure 11, thrombin formation took place in the distal region of the AAA, with the formation of more thrombin in case A than in case B [8].

This model couples fluid domains with chemical domains, which can aid in discovering the unknown mechanisms of ILT formation in AAAs and the risks associated with increased formation of ILT in AAA. In addition, the effect of ILT on wall stress is noteworthy. Some studies have shown that ILT formation is a natural positive response to aid in the protection against aneurysm rupture [9].

According to Mower et al., it is suggested that ILT presence on the aneurysmal wall can be helpful in providing some resistance against tissue failure or rupture [9]. ILT can contribute to reducing the applied stress at that location on the aneurysmal wall. Mower et al. used FEM to examine the effect of ILT on AAA wall stress. Their FEM model had the following assumptions: axisymmetric structure, no external forces or pressure effects, elastically deformed, homogeneous, and isotropic material behavior. The FEM model consisted of three concentric layers as shown in figure 12. ILT was introduced in the aneurysmal cavity [9].

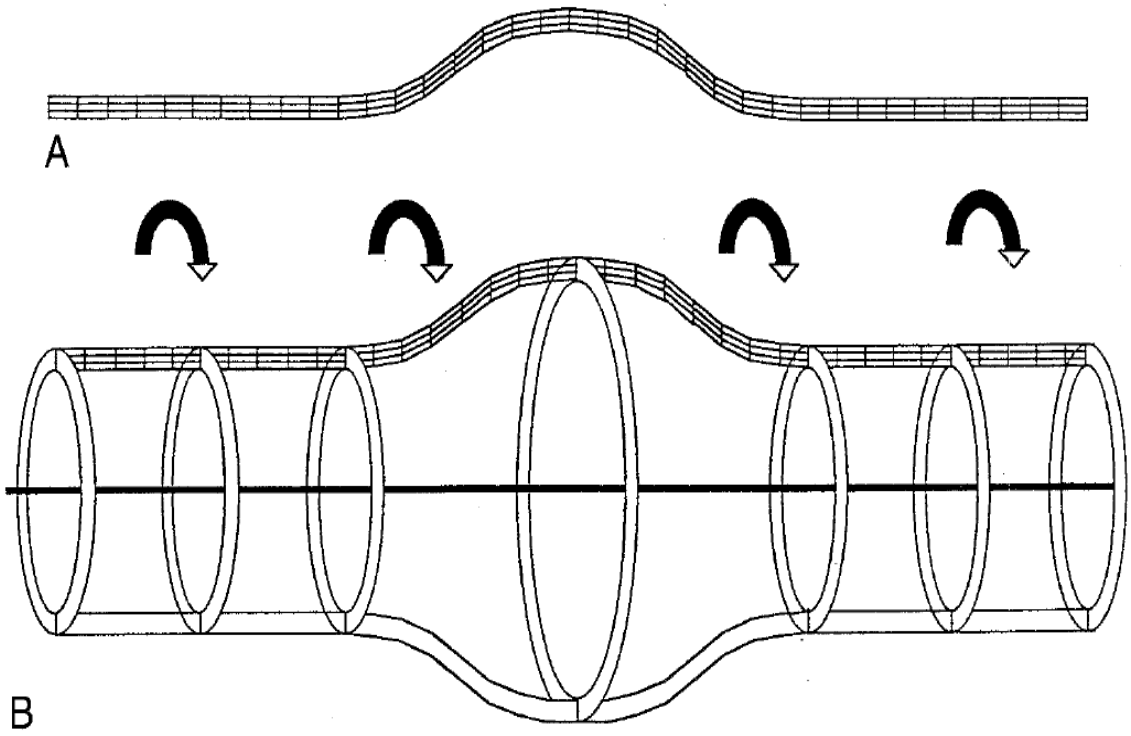

Figure 12 an axisymmetric finite element grid of a small aneurysm is shown in A. Rotation of the grid in A about an axis of symmetry generates the 3D structure shown in B [9].

ILT effects on maximum wall stress were observed by varying three parameters: relative thrombus depth (or thickness of ILT), thrombus elastic modulus, AAA wall elastic modulus for ILT elastic modulus of 0.02 MPa and 0.20 MPa, shown in figures 13 to 15, respectively [9].

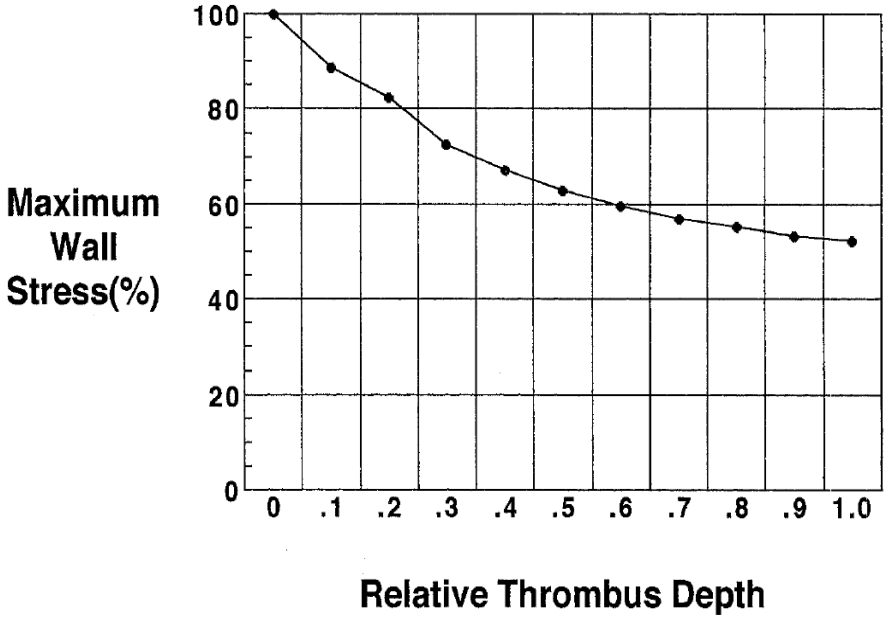

Figure 13 the size of the ILT helps in decreasing the maximum wall stress on the AAA's wall. Maximum wall stress is expressed as percentage of stresses in the aneurysm with no ILT and Thrombus depth is a fraction of the diameter [9].

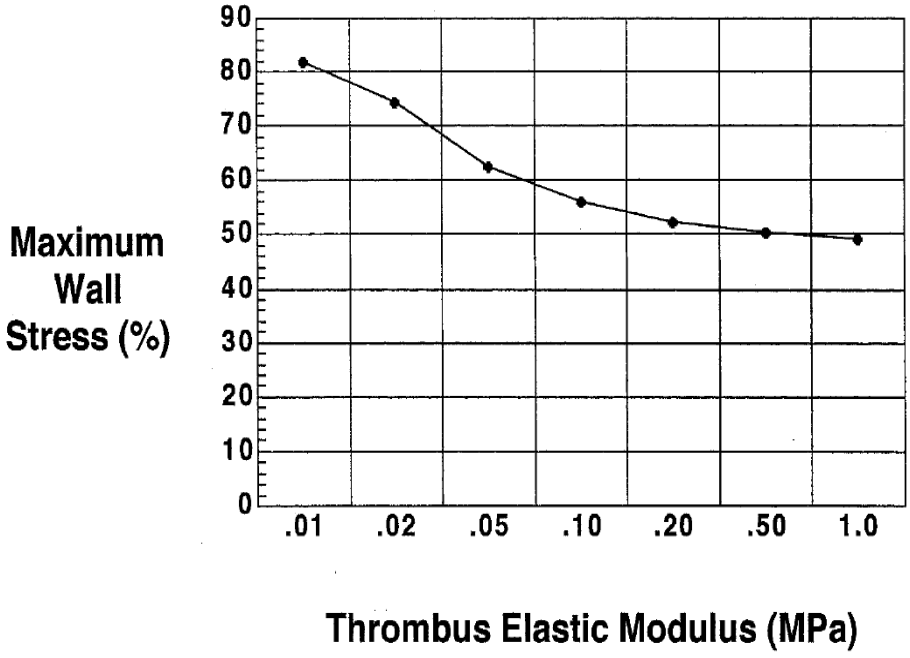

Figure 14 A decrease in maximum wall stress is observed as the elastic modulus (strength) of ILT increases. . Maximum wall stress is expressed as percentage of stresses in the aneurysm with no ILT [9].

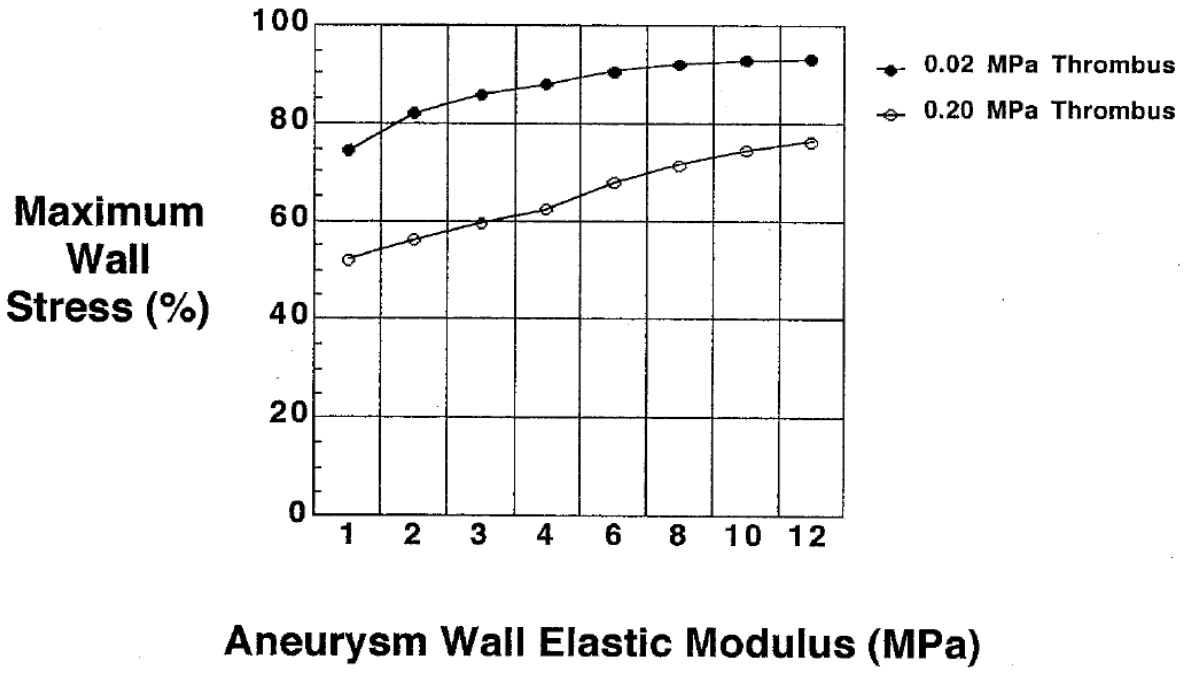

Figure 15 as the AAA's wall becomes stiffer, ILT is not able to absorb much of the stress, unless ILT has a high Elastic modulus. Maximum wall stress is expressed as percentage of stresses in the aneurysm with no ILT [9].

It is shown in the figures that the presence of ILT resulted in reducing the maximum wall stress applied on the AA wall by at least 30% for all three parameters [9]. Thus, it can be concluded that the presence of ILT can support the wall of AAA to some extent. Mower et al suggest that the formation of ILT is a natural response to protect against aneurysm rupture, because ILT absorbs the wall stress [9]. Also, they suggested that a larger ILT provides more protection as long as the relative size of the ILT is relatively small to the aneurysmal volume, and the protection decreases as the ILT size approaches the size of the aneurysmal cavity. However, the effect of ILT on blood flow and shear stress must not be ignored. The presence of ILT with a significant mass alters the nature of blood flow from laminar to turbulent flow. The presence of turbulent flow can cause elevated shear wall stress and ILT formation rate to increase [8].

Vorp and Geest demonstrated a patient-specific biomechanics approach to understand the process and to predict rupture in AAA patients [3]. They focused on the derivation of constitutive relationships via in-vivo mechanical testing and ex-vivo tensile testing. In-vivo imaging testing is non-invasive and is done via CT scans and ultrasound techniques. Such techniques are the most common in detecting AAAs via modeling of the aneurysm using FEM. Also, they help in detecting ILT via recording measurements of compliance. However, in-vivo imaging testing is not sufficient to derive the constitutive models for patient-specific local wall stress analysis. Rather, ex-vivo tensile testing is typically performed in order to derive constitutive equations. Vorp and Geest considered anisotropic properties for human abdominal aorta in their model [3]. Their work is the first to propose an anisotropic constitutive relation for AAA [3]. The effect of the presence of ILT on wall stress, the thickness effect of ILT on wall strength, and wall stress, strength, and RPI for patient-specific AAA are shown in figures 16,17, and 18, respectively.

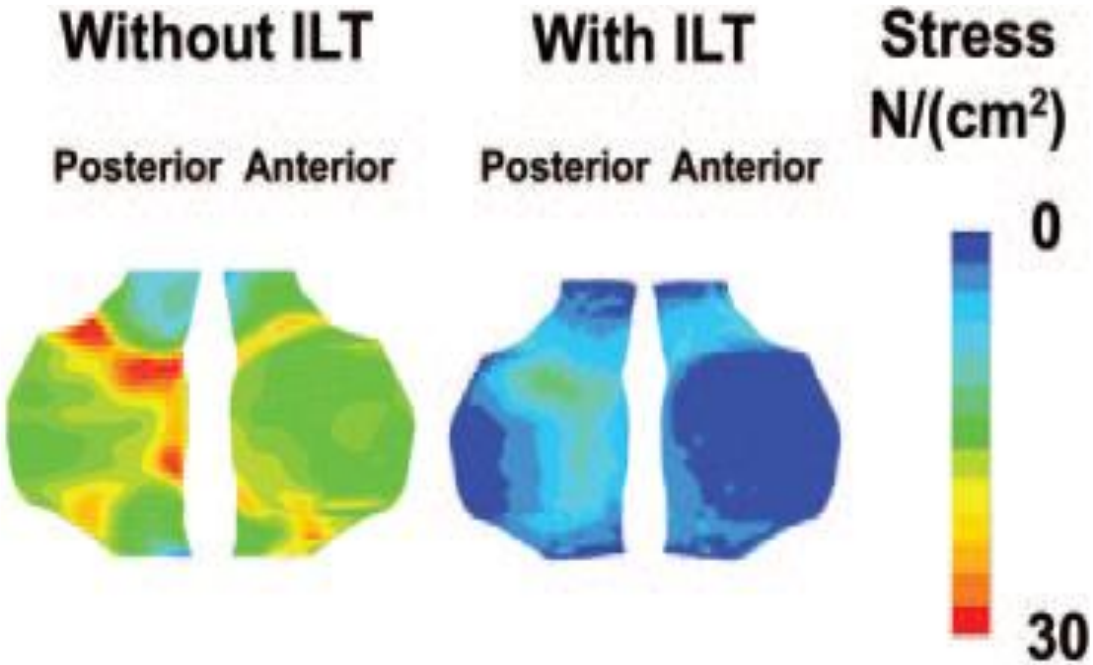

Figure 16. The effect on ILT on wall stress implies that ILT helps in reducing wall stress on AAA's wall [3].

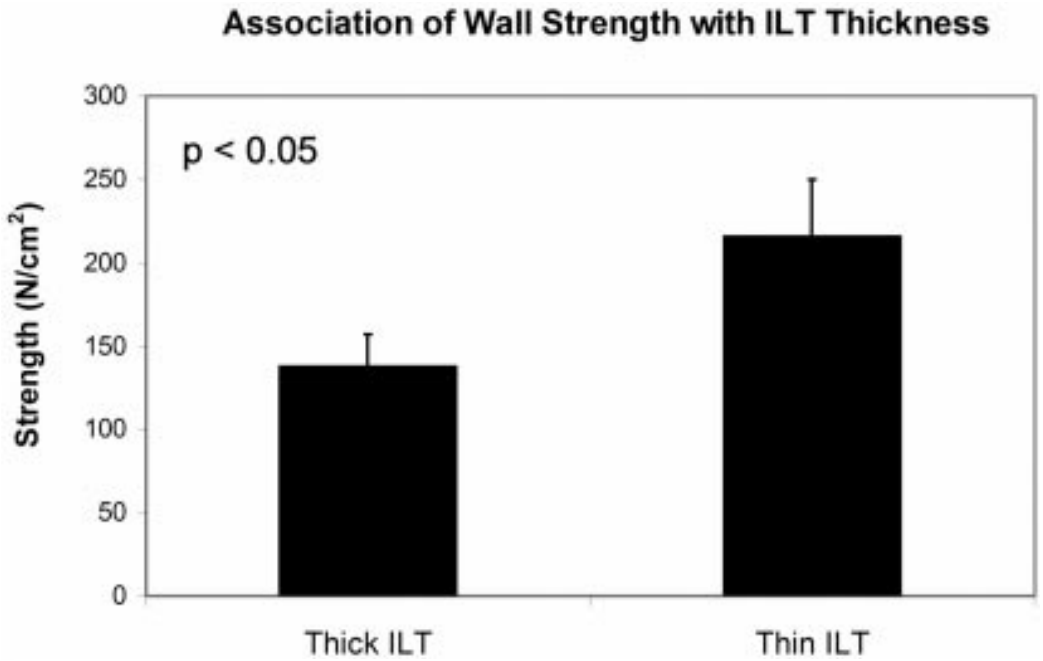

Figure 17 The presence of a thick ILT near the aortic wall reduces the strength of the wall compared to a thin or no layer of ILT near the aortic wall [3].

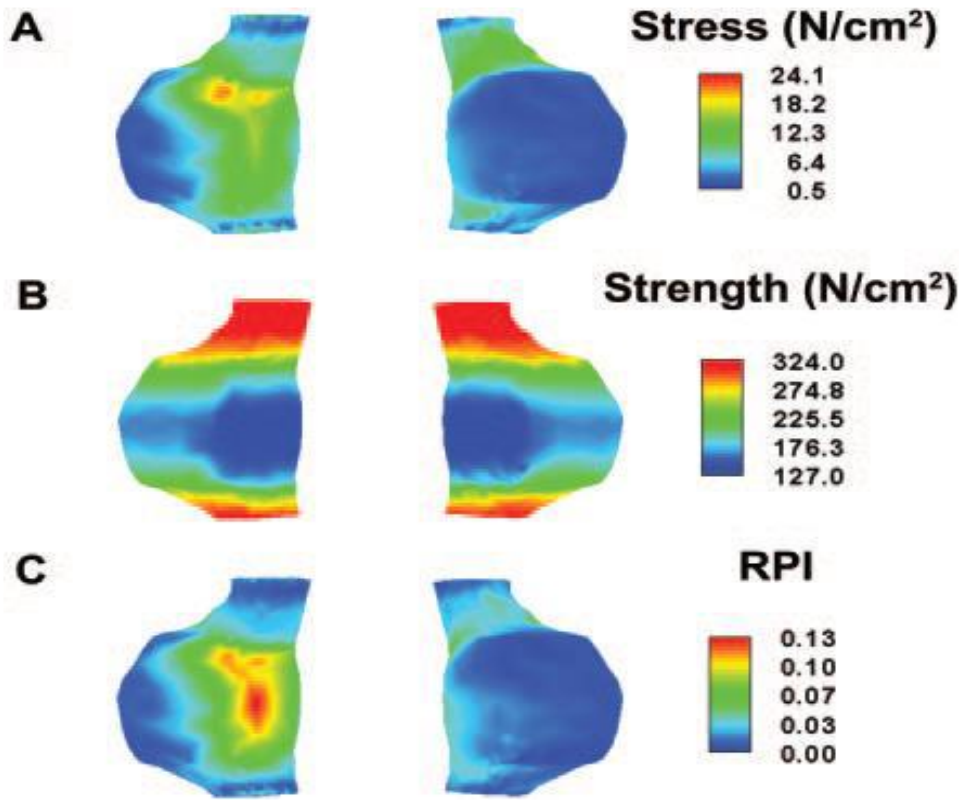

Figure 18 Wall stress (A), strength (B), and RPI (C) for a patient-specific AAA [3].

Vorp and Geest suggest that the presence of ILT in finite element analysis of AAA is essential for more accurate computations, because ILT can play a vital role in reducing wall stress, see figure 16 [3]. Thicker size ILT decreases the wall tensile strength, but thinner ILT increases wall tensile strength, refer to figure 9. Equation 5 was used to calculate the wall strength noninvasively depending on the patient's age, sex, smoking status, family genetic history of AAA, and size of AAA [3].

$$\boldsymbol{Strength = 141.26 - 17.16 * ILT + 3.39 * Age - 257.30 * Nord - 69.5 * Hist + \epsilon} \quad (\mathbf{5})$$

Where ILT thickness is measured in cm, age is in years, sex (male=0, female=1), smoking status (smoker=0, nonsmoker=1), family genetic history (with=1, without=0), size of AAA in cm [3]. The equation above was applied for a patient-specific AAA and the results are demonstrated in figure 10B. There is a need for biomechanical noninvasive techniques that measure wall stress, wall strength, and potential rupture site. The development of such techniques will aid in evolving a prognostic tool for clinicians to use.

Zelaya et al. suggested a linear approach model in order to improve the efficiency, effectivity, and ease of AAA wall stress computations, and, as a result, such models can be used as clinical tools for patient-specific wall stress assessments [10]. They developed three models to improve the relative accuracy of the linear approach used in computing AAA wall stresses: a reference model, a conventional model, and a proposed linear model, as shown in figure 19 [10].

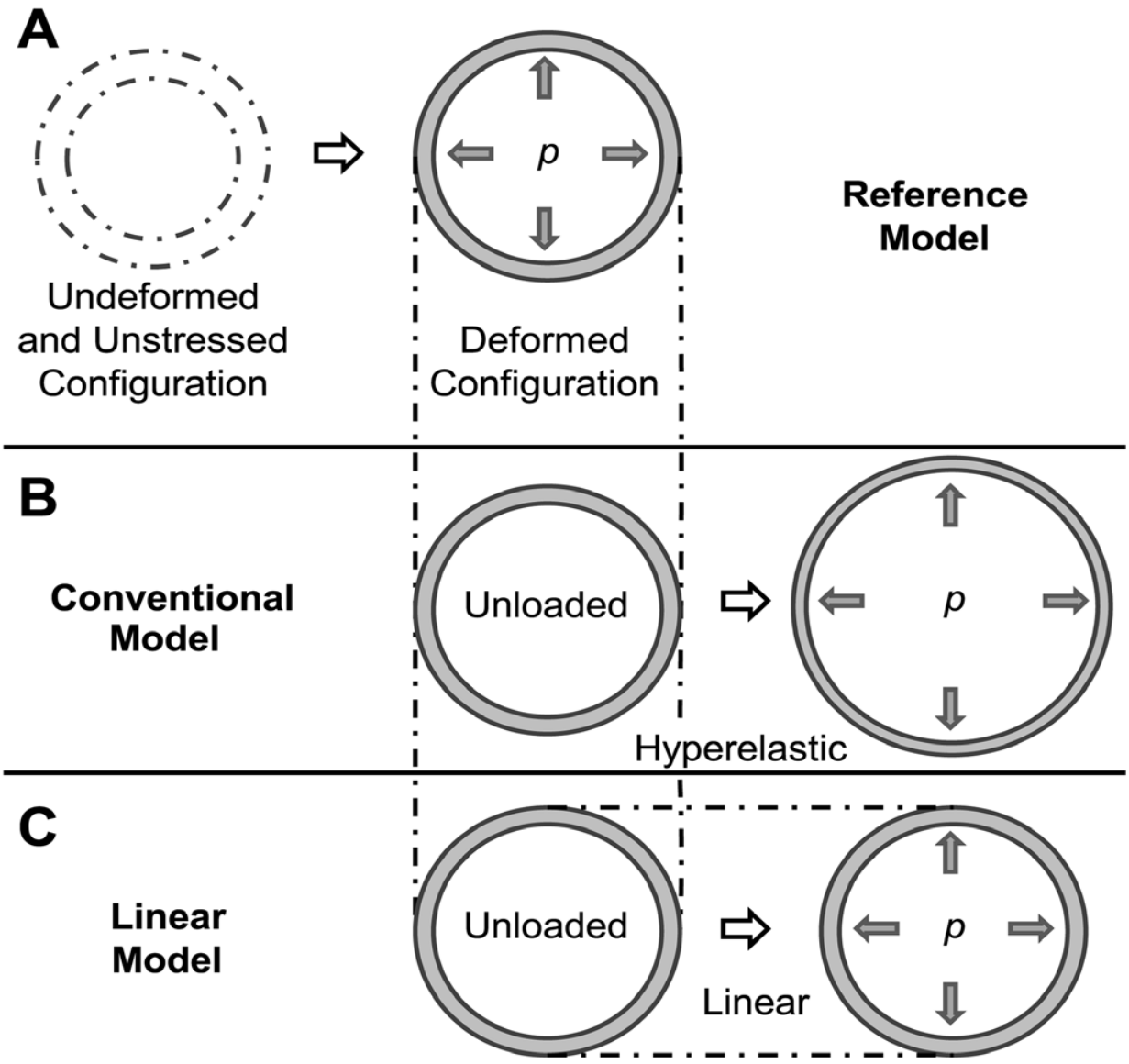

Figure 19 Three models were employed in the study. The deformed configuration of the reference model is the initial configuration for conventional and linear models. For (A & B) models, the walls are hyperelastic with nonlinear behavior. For (C) model, the walls are linear elastic in properties, with infinitesimally small deformations and strains [10].

For all the models proposed, the equations of equilibrium were used and solved with the boundary conditions as shown in the equilibrium equation below [10]:

$$\boldsymbol{\nabla . \sigma = 0} \qquad \boldsymbol{in\ \Omega} \qquad (\mathbf{6})$$

Where σ is the Cauchy stress tensor, Ω is the body domain in the deformed configuration.

Boundary conditions shown in equations 7.

$$\boldsymbol{\sigma . \hat{n} = -p\hat{n}} \qquad \boldsymbol{on\ \Gamma_l} \qquad \textit{and} \qquad \boldsymbol{\sigma . \hat{n} = 0} \qquad \boldsymbol{on\ \Gamma_0} \qquad (\mathbf{7})$$

Where $\hat{n}$ a unit vector is normal to the wall surface, p is the intraluminal systolic pressure which is 120 mmHg (0.016N/mm^2), Γ_l is the lumen surface of the deformed configuration, Γ_o is the outer surface of the deformed configuration.

Equation 8 is an energy density function, W, for an almost incompressible, homogenous, and isotropic AAA wall properties:

$$\boldsymbol{W} = \alpha(\mathbf{I_B} - 3) + \beta(\mathbf{I_B} - 3)^2 + \gamma(\mathbf{I_B} - 3)^3 \qquad (8)$$

Where $\boldsymbol{\alpha, \beta, \& \gamma}$ are coefficients that denote the properties of the tissue are, $\mathbf{I_B}$ is the first invariant of the left Cauchy-Green Tensor **B** ($\mathbf{I_B} = \boldsymbol{tr}\mathbf{B}$) with$\mathbf{B} = \boldsymbol{FF^T}$; F is the deformation gradient tensor.

Equation 9 represents a constitutive relation for nonlinear material.

$$\boldsymbol{\sigma} = -H\mathbf{I} + 2\frac{\partial W}{\partial \mathbf{I_B}}\mathbf{B} \qquad (\mathbf{9})$$

Where **H** is the hydrostatic pressure, and **I** is the Identity tensor.

The following assumptions were made for the linear model: almost incompressible, linear and elastic material, and high Young's modulus. The constitutive relation is expressed in equation 10.

$$\boldsymbol{\sigma} = \mathbf{C}\boldsymbol{\varepsilon} \qquad (\mathbf{10})$$

Where C is the stiffness tensor, for an isotropic material C depends on E and Poisson's ratio υ, ε is the infinitesimal strain. E=8.4*10^9 N/mm^2 and $\upsilon = 0.4999$ were used for the linear model [10].

Initial configurations and material properties were different among the three models. The initial configuration of the reference model was the unstressed and unloaded configuration of the tissue. For the conventional and linear models, the initial configuration is the deformed configuration of the reference model [10].

Figure 20 shows a thick wall cylindrical model with applied internal pressure, and no stress or load is applied in the undeformed configuration. However, internal pressure exists in the deformed configuration [10].

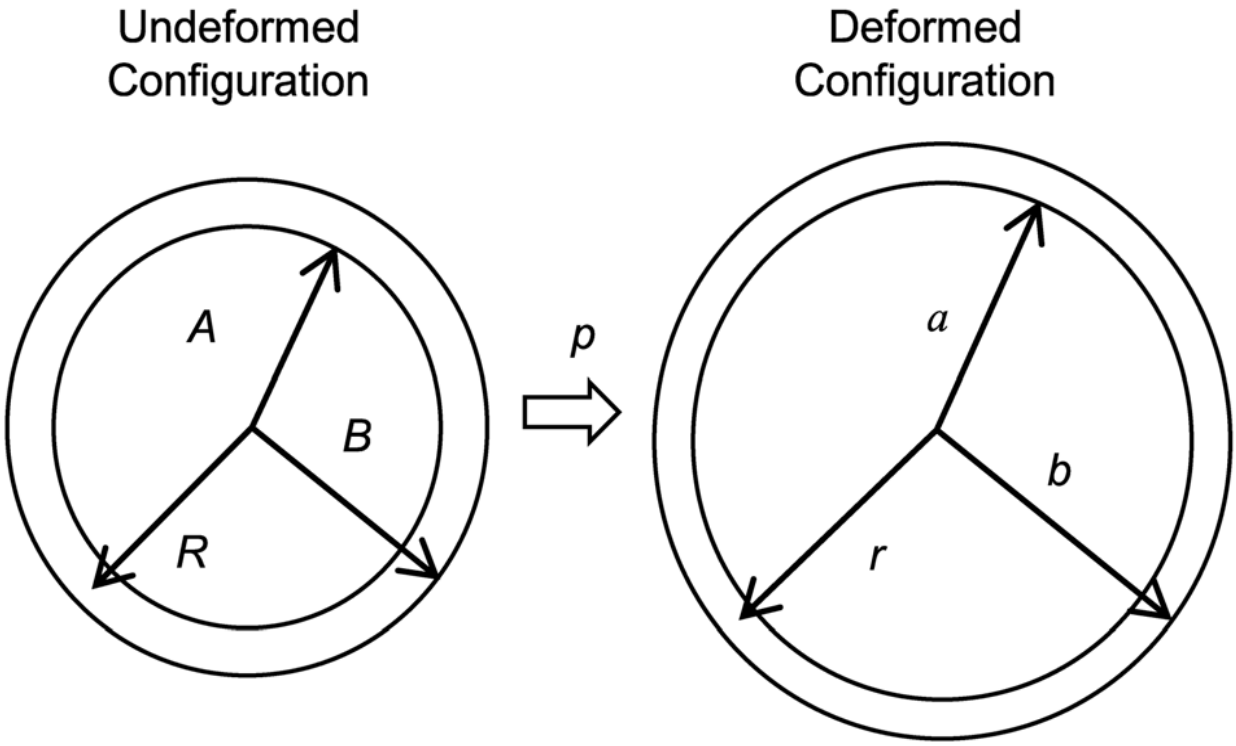

Figure 20 shows the deformed configuration once an internal pressure is applied. A represent the internal wall radius, B represents the external wall radius, and R represents the radial wall coordinate. Where a, b, and r represent the same thin, but in the deformed configuration [10].

Figures 21 and 22 show effective stress results obtained using the three different models and the relative difference in effective stress between the linear and conventional model:

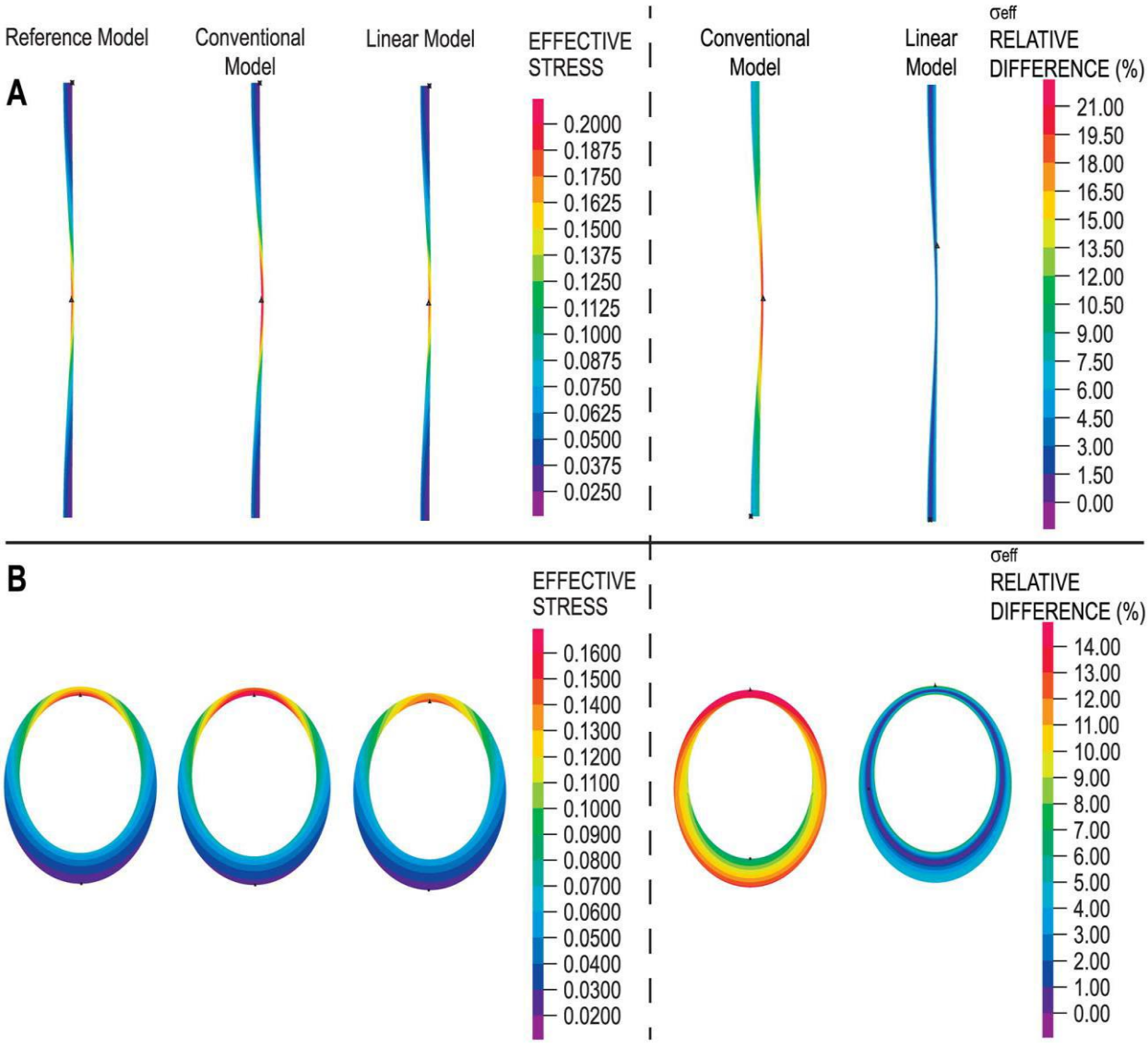

Figure 21 shows the effect of variable wall thickness on wall stress distributions using all three models. A is an axisymmetric model with longitudinally-varying wall thickness, where B is a plane strain model with circumferentially varying wall thickness [10].

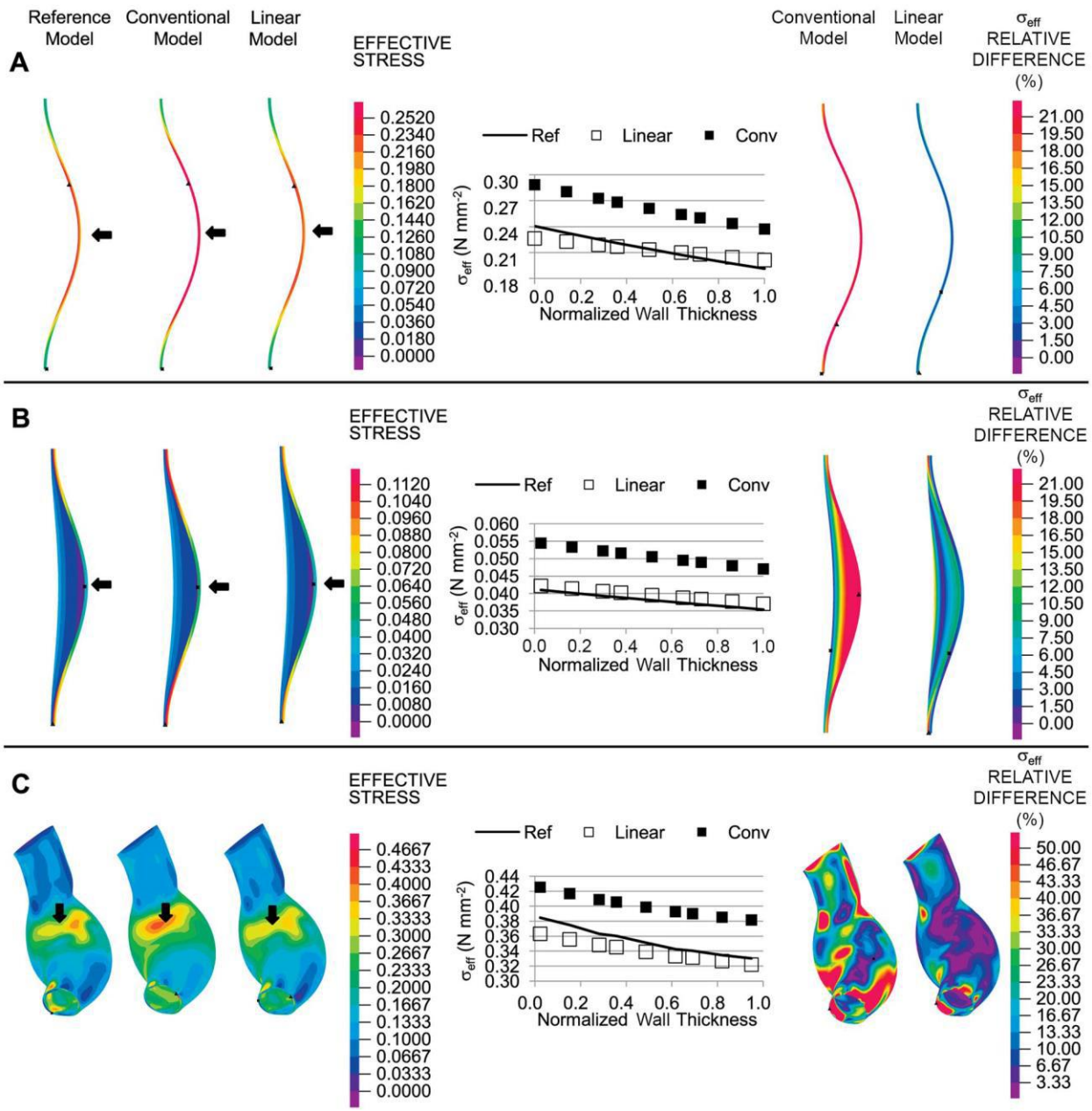

Figure 22 shows the effect of different geometries of AAA on wall stress distributions using all three models. A is an axisymmetric model, B is an axisymmetric model with ILT, and C is a patient-specific model [10].

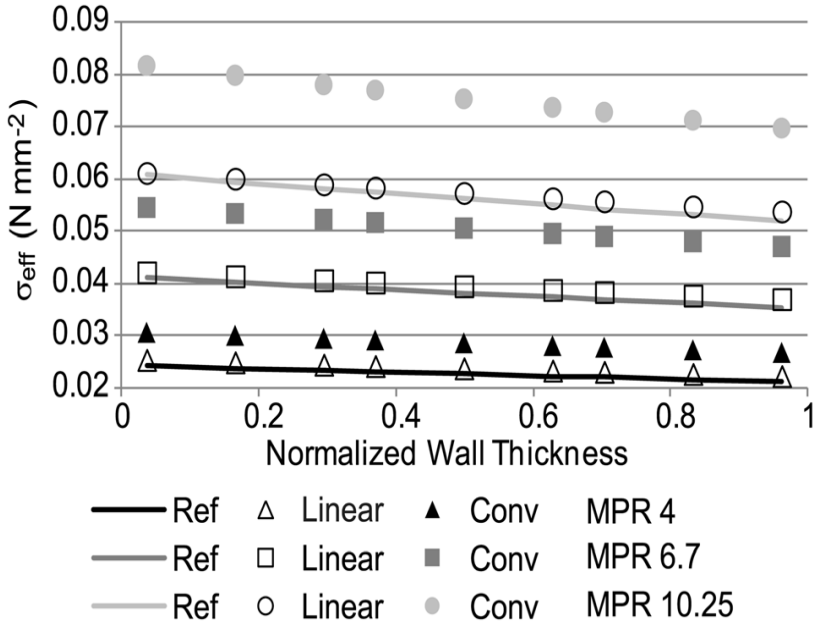

Figure 23 shows the effect of wall/thrombus material property ratio (MPR) on the effective stress distributions [10].

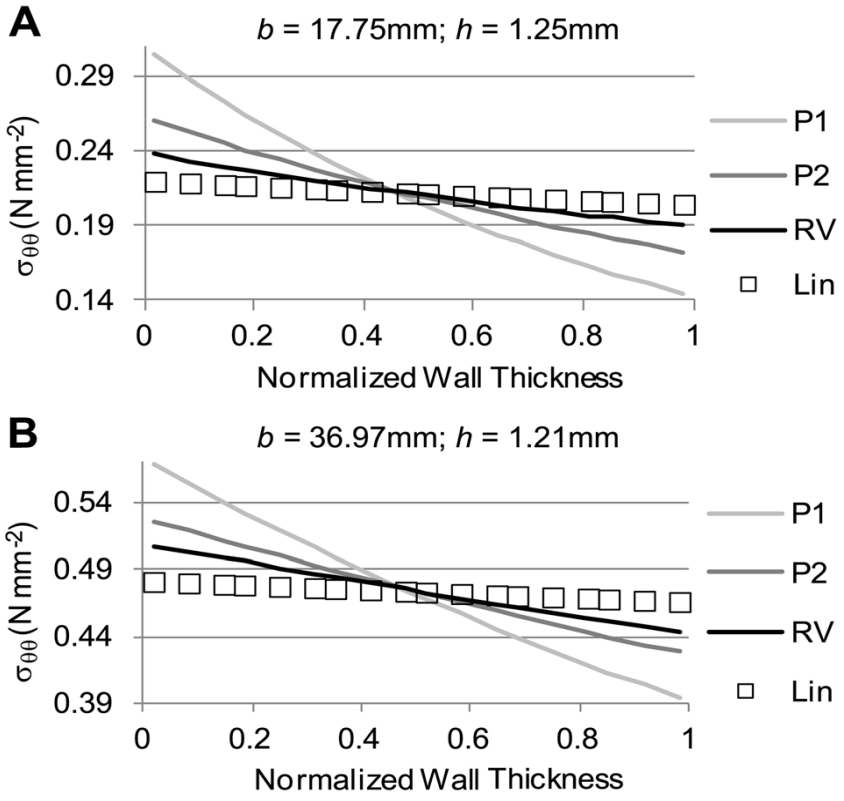

Figure 24 shows a comparison of circumferential stress distributions using the different tissue properties values shown in table 1 above (RV, P1, & P2), and results using the linear model (Lin). (A) is a small aneurysm, where B is a bigger aneurysm [10].

Zelaya et al. concluded that their linear approach can be used to accurately approximate wall stresses for various geometries with different material properties, which makes their model easy to use as a clinical tool for measuring and analyzing patient-specific wall stresses [10]. When comparing the linear model with reference model, figure 21, the linear model demonstrates closer approximations of stress values to the reference model. Thus, Zelaya et al. suggests that the linear approach can be a better accurate tool to measure wall stresses and effects of wall thickness than the conventional model [10].

Zelaya et al. accounted for curvature in their models. They constructed an axisymmetric, curved wall aneurysms subjected to internal pressure at the interior [10]. They found that higher stresses are found at walls with higher curvature, figure 22A. Also, they considered the effect of ILT on wall stress, figure 22B. They assessed the effect of complex curvature and asymmetry in an aneurysm. They considered patient-specific AAA and applied the models to approximate wall stresses, Figure 22C. In all of the aforementioned cases, the linear model had closer approximations to the reference model. This finding indicated that the linear model is a more accurate model in computing wall stresses for various geometries of AAA, and provides desirable physiological wall stress profile over the wall thickness [10].

Realistically, aneurysms are not usually symmetrical, and it is important that modeling methods account for that fact. Considering asymmetry in modeling methods will allow us to compute more accurate values of stresses and strains, and, eventually, improve the assessment of rupture site in the aneurysm.

The expansion of AAA's wall is not usually symmetrical overtime. Most of the aneurysms exhibit asymmetric and complex geometrical shapes. The bulge shape and diameter of the AAA may have an effect on wall strength and risk assessment [11]. Vorp et al. focused on studying AAA wall stress distribution due to the effects of AAA bulge and diameter, as shown below [11].

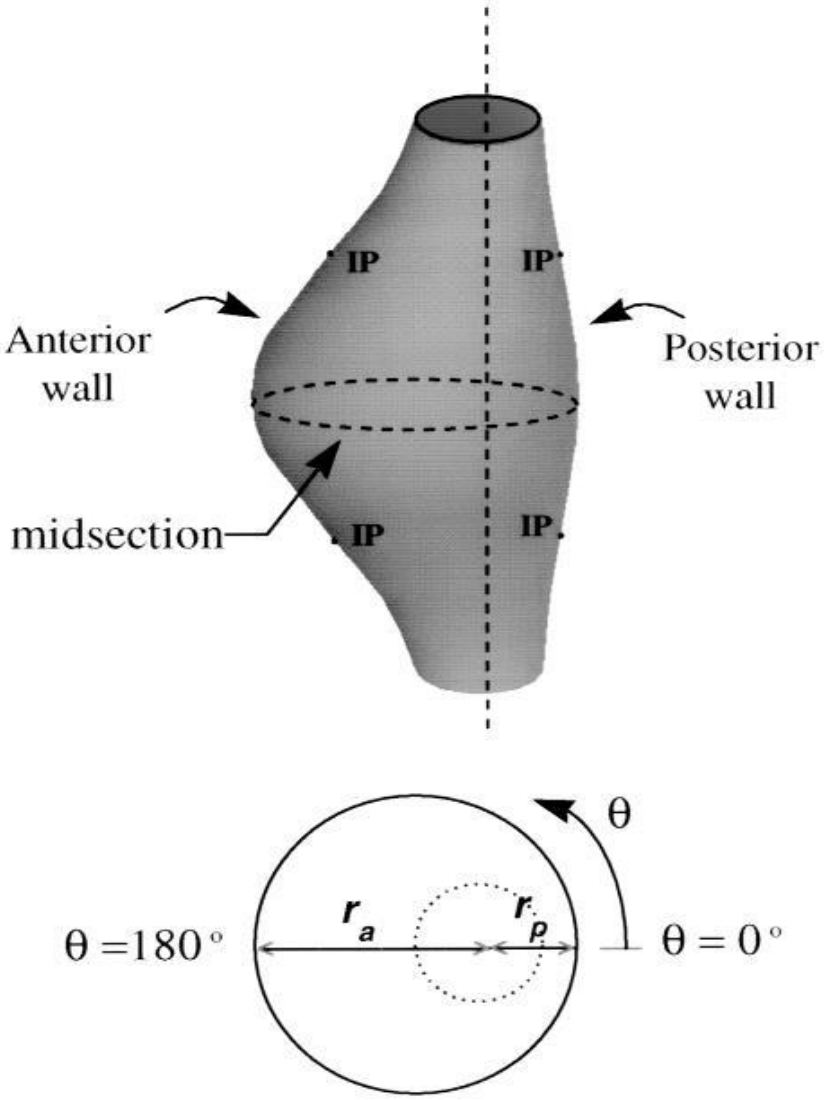

Figure 25 shows a 3D model of an AAA, where r_a is the maximum anterior wall dimension, and r_p is the maximum posterior wall dimension. The vertical dashed line passes through the center of the undilated inlet and outlet. Inflection points (IP) indicate the points at which the concavity of the wall changes from outward to inward and vice-versa [11].

Vorp et al. constructed a 3D hypothetical aneurysm using computer software. Varying wall thickness was not considered in the study, since the main focus is on symmetry, asymmetry, and maximum diameter of the bulge [11].

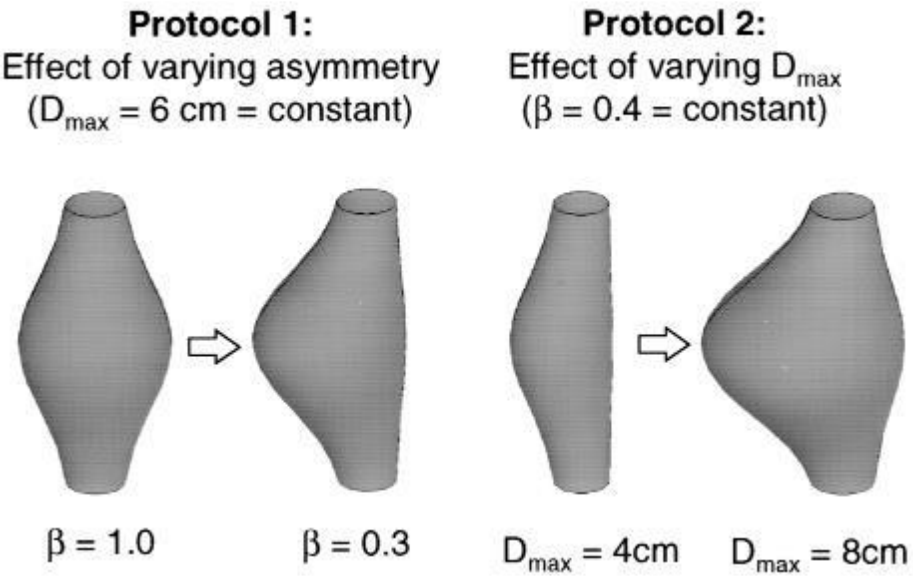

Figure 26 shows two cases, varying the asymmetry under constant maximum diameter (fusiform and saccular aneurysms) and varying maximum diameter [11].

Each modeled aneurysm was 12 cm long (z=0, superior end, and cm to z=12 cm, inferior end), where z= 6 cm is the midsection. Wall thickness of the aneurysms generated above was kept constant and uniform at 1.5 mm, $D_{max} = r_p + r_a$, and $\beta = r_p/r_a$. The analysis was done using finite element techniques. ANSYS finite element software was used to discretize each aneurysm into small linear elastic, quadrilateral shell elements. The total number of total elements ranged from 3200 to 3800 depending on the structure of each constructed aneurysm [11]. The wall tissue was assumed to be incompressible, the applied internal pressure was 120 mmHg (1.6 N/cm^2), the shear stress was neglected due to its small values compared to large wall stress values, the elastic modulus of the tissue was E= 500 N/cm^2, and the Poisson's ratio was v=0.49 [11].

The results of the 3D analysis of wall stress distribution for a total of 10 constructed aneurysms (5 with constant maximum diameter and 5 with constant symmetry) are shown below.

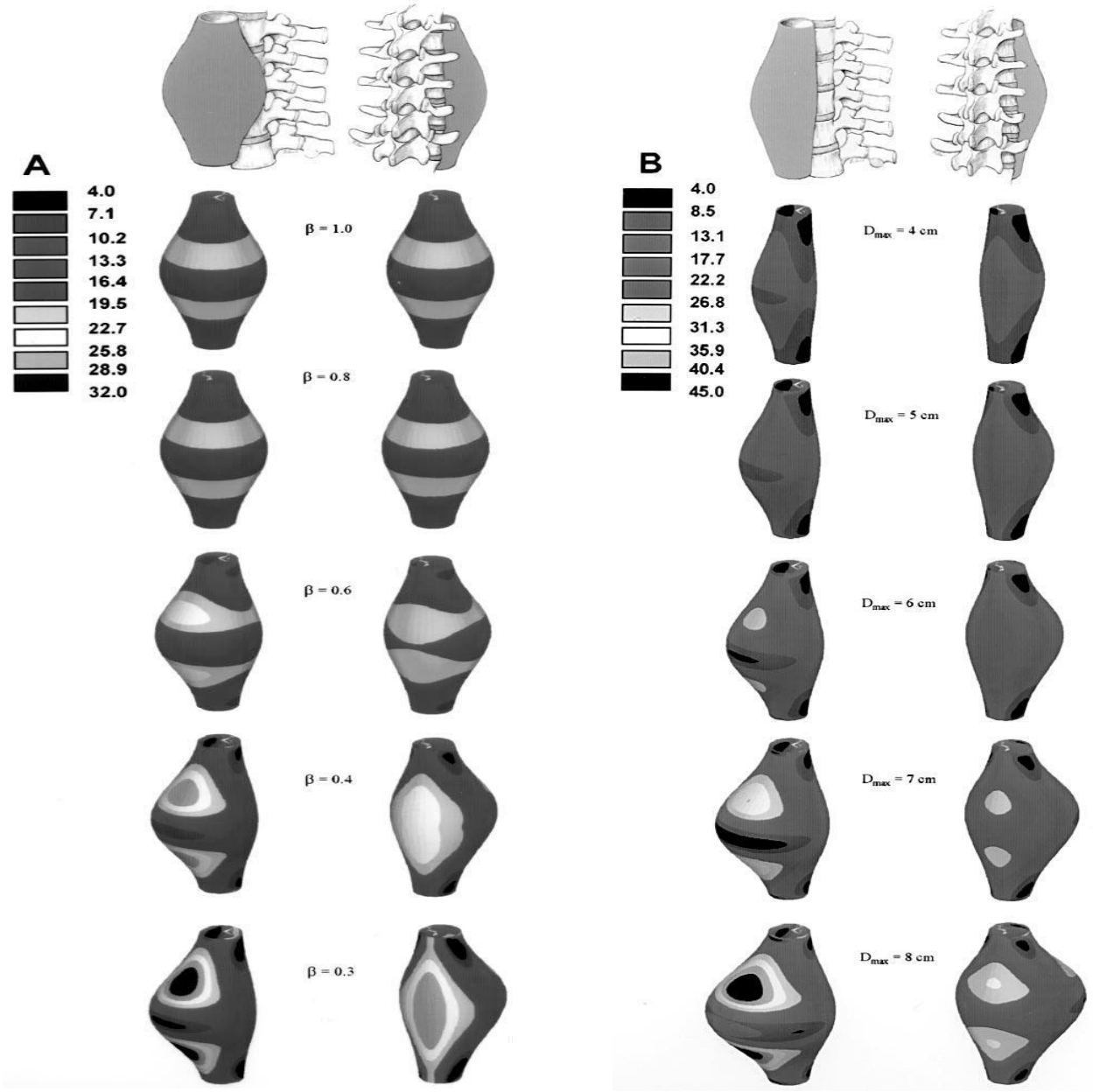

Figure 27 shows distribution of mechanical wall stress for all 10 aneurysms. For A, the symmetry is varied, and for B, the maximum diameter is varied. The left columns of A and B show the anterior surface of the aneurysm, where the right columns of A and B show the posterior surface of the aneurysm. The anatomic reference is shown above where the aneurysm is attached to the vertebrate column. The color scales on the side represent the magnitudes of wall stress (in N/cm^2) [11].

The effects of asymmetry and maximum diameter on the circumferential wall stress distribution and longitudinal wall stress distributions at midsection, anterior, and posterior surfaces are shown in figures 19, 20, and 21, respectively [11].

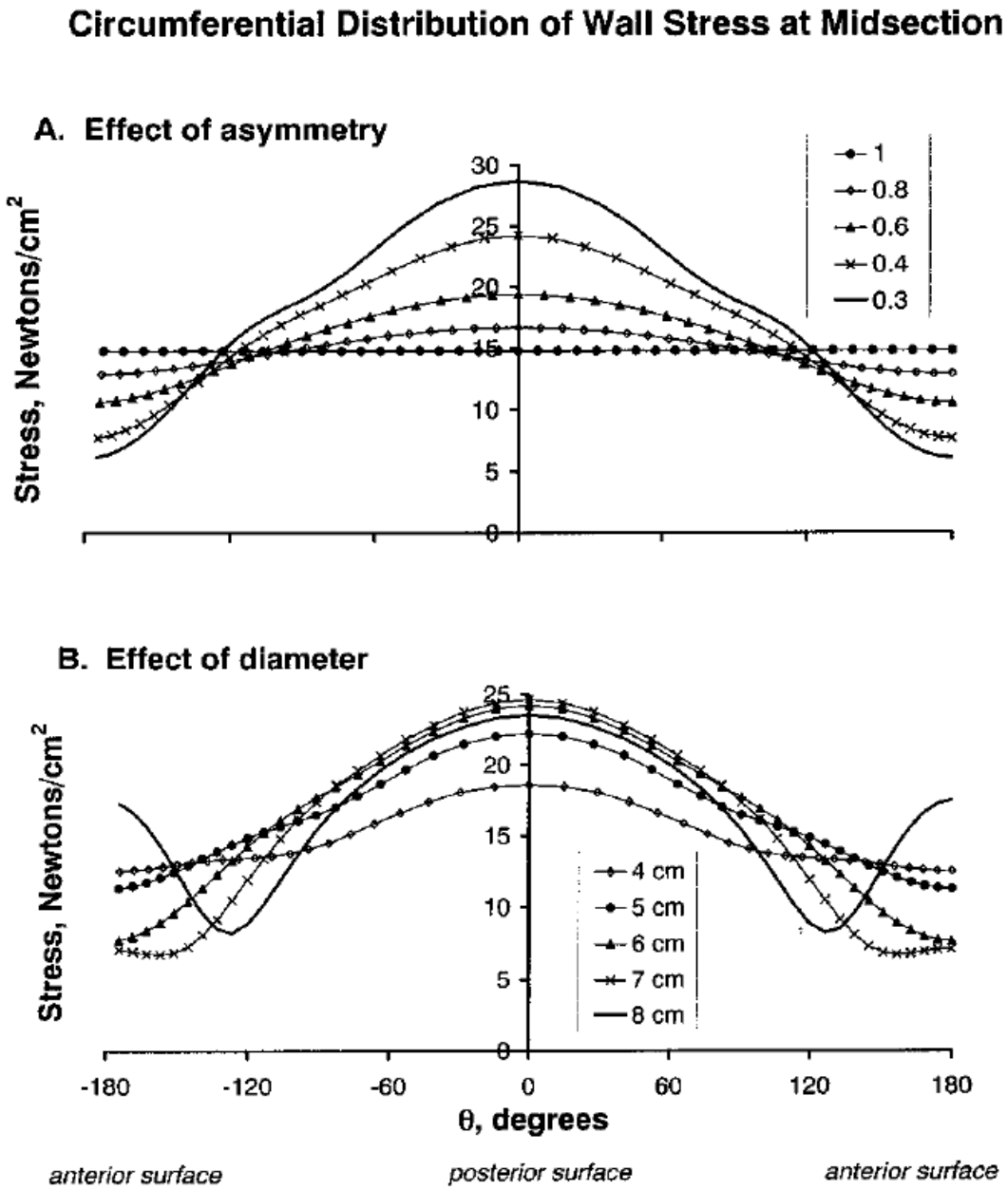

Figure 28 shows A, effect of symmetry, and B, effect of maximum diameter, on the circumferential wall stress distribution starting from the posterior position and ending in the anterior position along the angle theta of the midsection of each aneurysm, as shown in figure 24 [11].

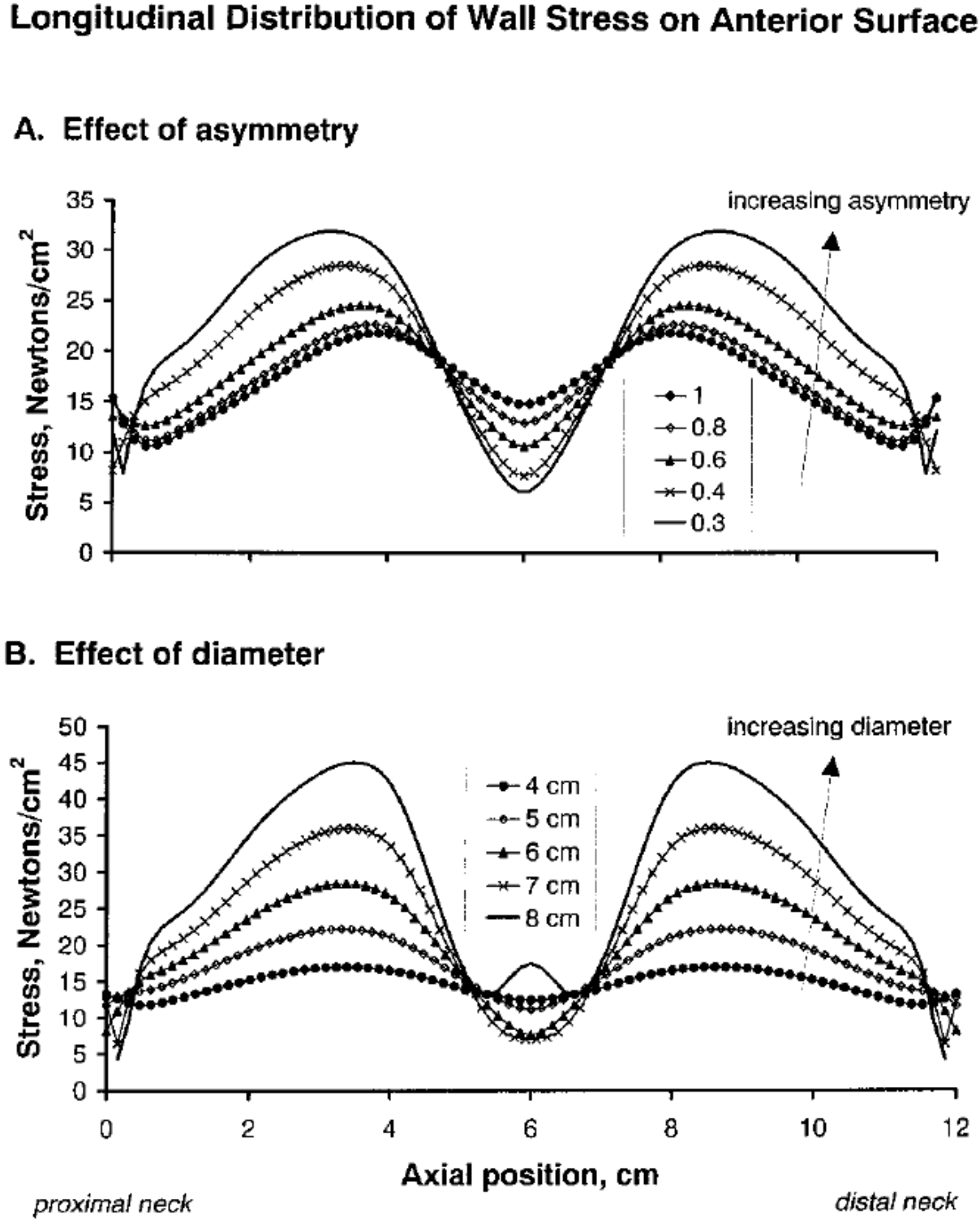

Figure 29 shows A, effect of symmetry, and B, effect of maximum diameter, on the longitudinal wall stress distribution on the anterior surface, starting from z= 0 cm, superior end, to z=12 cm, inferior end, and z= 6 cm is the midsection [11].

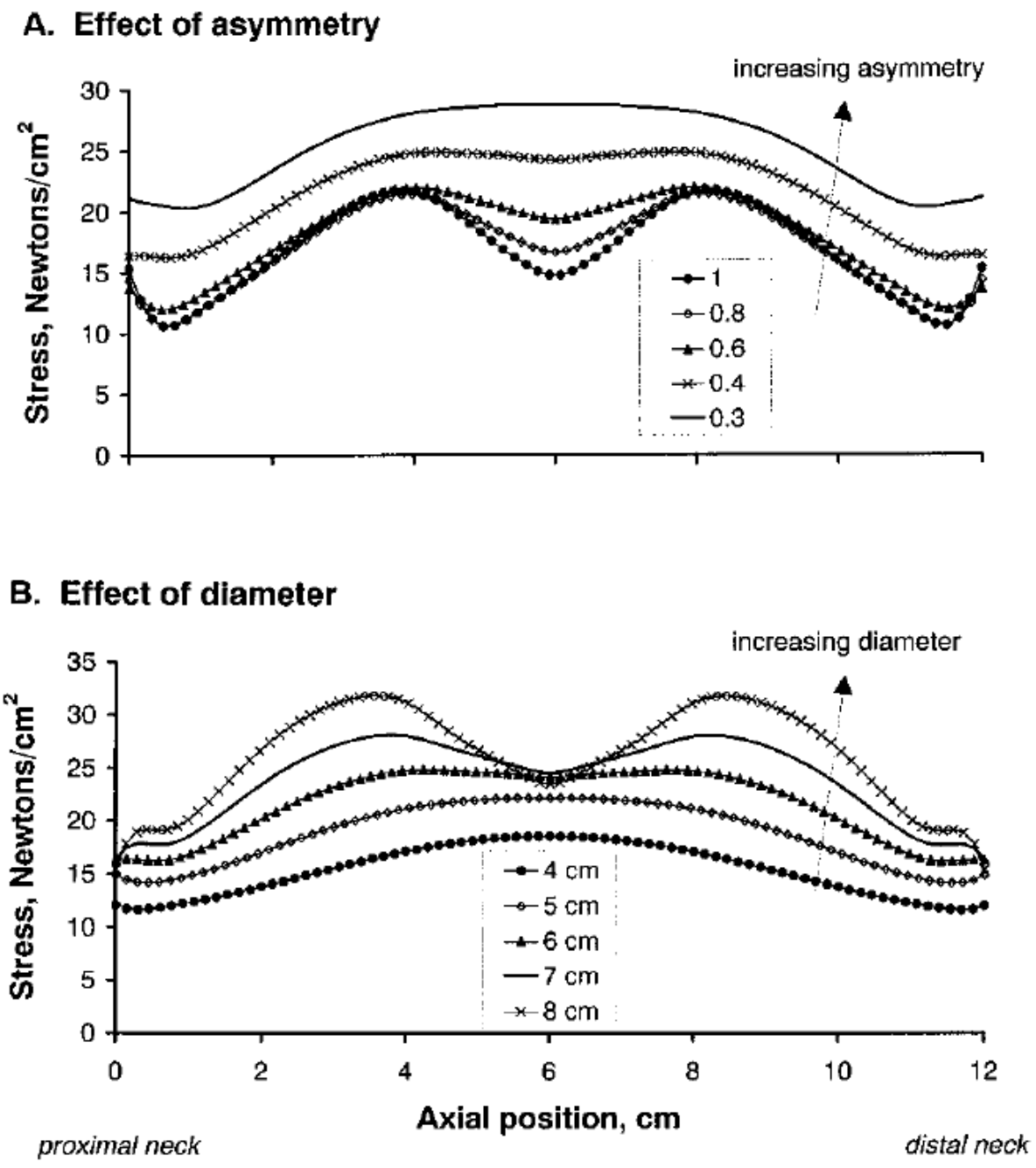

Figure 30 shows A, effect of symmetry, and B, effect of maximum diameter, on the longitudinal wall stress distribution of the posterior AAA's surface, starting from z= 0 cm, superior end, to z=12 cm, inferior end, and z= 6 cm is the midsection [11].

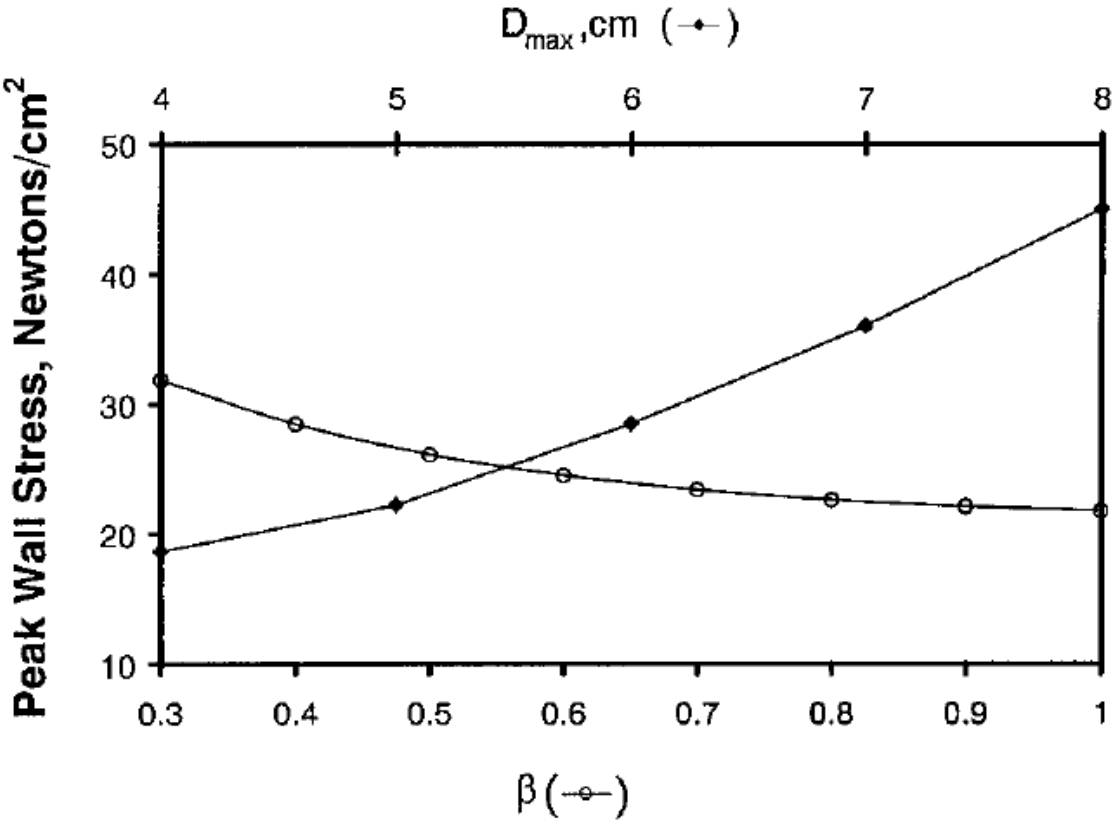

Figure 31 shows the effect of increasing diameter and asymmetry on the peak wall stress constructed AAA [11].

Based on the results of the study, it was observed that different shapes of AAA experience different wall stress distributions, in which, some maybe at higher risk than the others depending the values of the wall stress in each AAA. However, this study is not sufficient to conclude whether the maximum wall stress is always at the midsection, where the maximum diameter is, or else where within the aneurysm, or whether the most bulging aneurysm is at a higher rupture risk than the less bulging aneurysms. On the other hand, it can be concluded that an increase in maximum diameter and asymmetry will increase the risk of rupture over all [11].

Chapter 3

Purpose of Study

Goals and Objectives

- Develop the capability to simulate the deformation of the aorta walls during progression of AAA that requires:
    - Capability to conduct finite element analysis of pipes made from soft tissue to determine
        - Stress and strain in the region of the aneurysm
        - How they are affected by variables such as collagen degradation
    - Develop/identify accurate constitutive relationships between stress and strain for large deformations
    - Develop a rupture criterion

Hypothesis

Collagen degradation causes a change in the average Elastic Modulus (E_{avg}) in aortic tissues, which ultimately leads to the development and rupture of abdominal aortic aneurysms.

Aims

- Study, observe, and develop stress-strain relationships in healthy and collagen degraded abdominal aortic specimens
- Model the growth of AAA from an initial stage of the disease progression via conducting finite element analysis on an aneurysmal aortic model.

Chapter 4

Mechanical Testing and Modeling Approach

Problem

Abdominal Aortic Aneurysm (AAA) is the bulging or abnormal expansion in diameter of the abdominal aorta (the region of the aorta directly below the renal arteries and directly above the bifurcation point to the femoral and iliac arteries). If AAA is left untreated, then there is a high risk of rupture. If rupture occurs, then the person's life is at risk if not hospitalized immediately. One of the current challenges that physicians face is detecting the rupture site of the aneurysm accurately due to the lack of good prognostic tools that help them in anticipating the rupture site and develop a treatment plan for the patient. Such a prognostic tool must be able to model the rupture criteria via measuring the rate of growth of the aneurysm, determining how the tissue properties change with time and growth of the aneurysm, predicting rupture site based on changes in such properties, and ultimately to be able to give a better understanding of disease progression.

AAA Model

In order to study the problem and be able to contribute to development of a prognostic tool for detecting and predicting rupture site, it is important to define the biological forces present, model the growth of the aneurysm, and model the dynamics of blood-tissue interaction. Such an approach will allow us to study the stress-strain relationships of the deformed aneurysmal aortic wall, the laminar vs. turbulent flow in the aneurysm and how it affects the shear stress on the wall of the aorta, and the effect of turbulent flow on the formation of intraluminal thrombus on the aortic aneurysm wall. Finite element analysis and computational fluid dynamics are computer-based modeling tools that aid in the study of stress-strain relationships on tissue models, and fluid-structure analysis on blood vessel-like models. Good

representation of material properties representative of the aortic wall tissue is an important aspect of developing a prognostic tool.

Mechanical Testing

In this study uniaxial testing of healthy longitudinal and circumferential abdominal aorta (AA) specimens and collagen degraded ("aneurysmal") longitudinal and circumferential AA specimens was performed, as shown in figure 32.

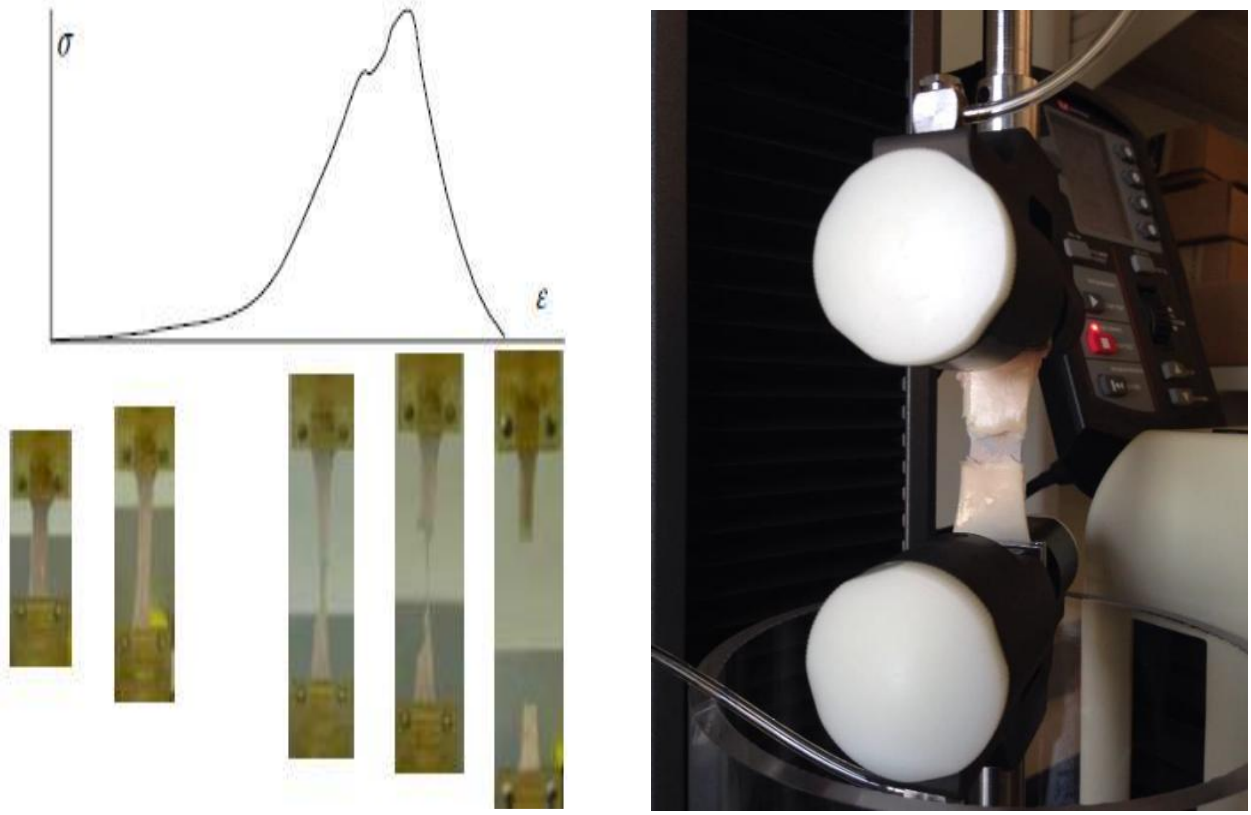

Figure 32 shows the deformation stages the specimen until rupture takes place (left) and one of our specimens rupture point after uniaxial testing was performed (right).

Instron 5944 machine was used for all the mechanical testing performed. The Instron was equipped with a Bioplus bath where testing can be performed under environmental conditions that resemble the soft tissue in vivo environment. The mechanical tensile test was performed based on strain rates of 1, 0.1, 0.01, 0.001 mm/mm/min. For every strain rate, the mechanical test was carried in two steps: (a) 5 cycles of hysteresis for each specimen for up to 20% strain, and (b) tensile test until rupture.

Abdominal aortic specimens were obtained from pigs (5 months, 200 lb.). Certain sections of the aorta were cut vertically to obtain a longitudinal orientation and some sections were cut horizontally to obtain a circumferential orientation. Each specimen had a length of 5-7 cm, width of 2-2.5 cm, and thickness of approximately 1.5-2 mm. The specimens were frozen at in the – 80 ^{0}C freezer, and, prior to mechanical testing, the specimens were removed from the freezer to thaw at room temperature for 12 hours. Then, the specimens were mounted on the Instron machine and were left to sit in the Bioplus bath, which contains saline solution (1X PBS), at 37 ^{0}C for 30 minutes before performing the mechanical tests.

Collagen degraded abdominal aortic specimens were immersed in collagenase solution for 24 hours prior to mechanical testing. The collagenase solution had a concentration of 0.11 g/ml, and was made via mixing of collagenase powder with 1X HBSS (Hank's Balanced Salt Solution). Specimens were placed in a fresh collagenase solution prior to every test performed. All collagen degraded specimens tensile testing was performed at a strain rate of 1 mm/mm/min.

The following was observed from the data collected: The relationship between stress and strain, elasticity of healthy and collagen degraded specimens, and the age corresponding to the specimens based on actual AAA donors' data reported in the literature. A mathematical model from Ranghaven et al. was applied in this study [5]. The model is shown in figure 33:

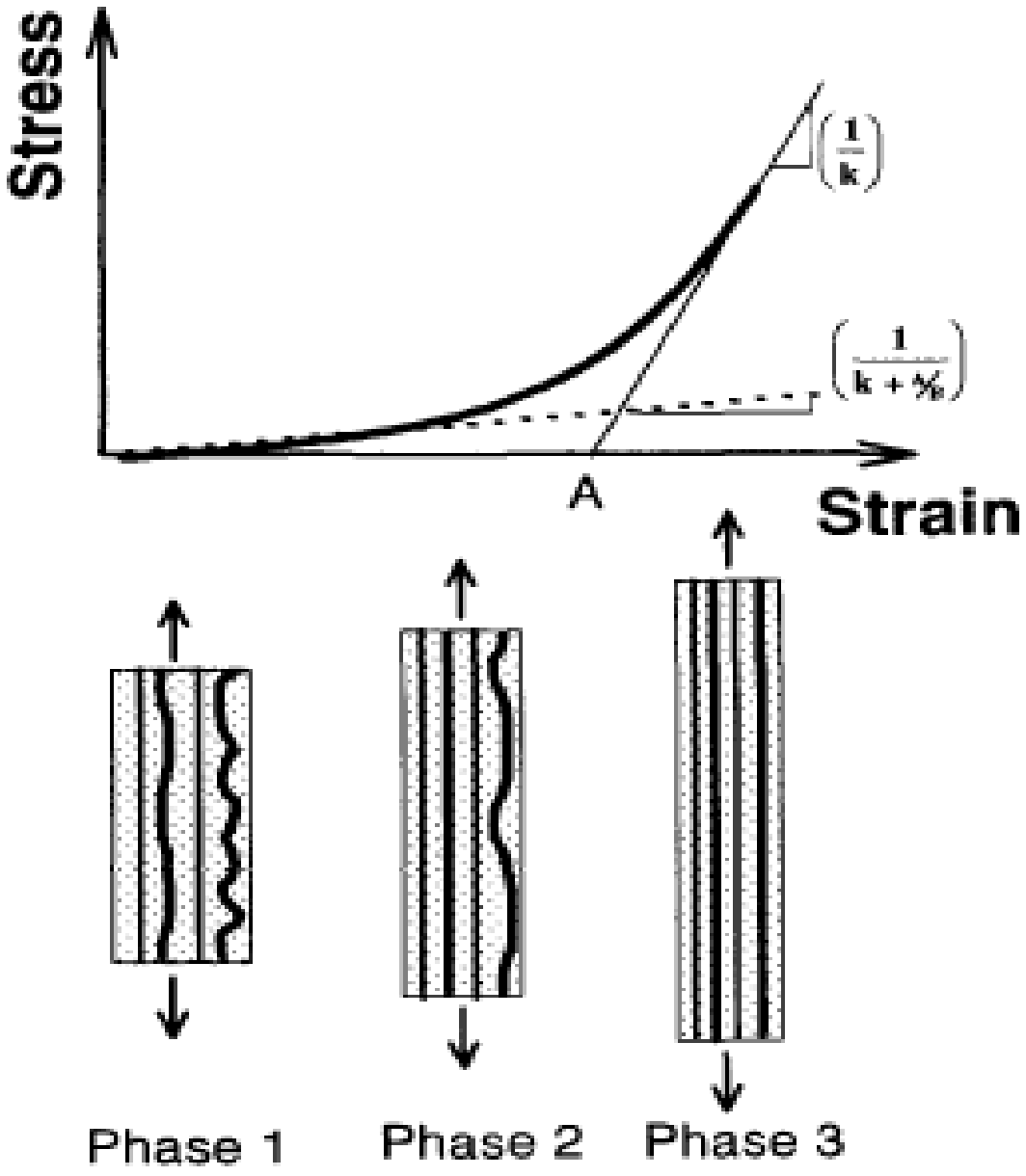

Figure 33 the stress-strain model relationship per phase. Phase 1 involves elastin support, Phase 2 involves the onset of collagen fibers support, and Phase 3 involves all collagen fibers support. On the right, the equations that describe the elastic modulus of each phase [5].

According to Raghaven et al. [5], equations 11-13 express the mathematical relationship between stress and strain.

$$\left.\frac{d\sigma}{d\varepsilon}\right|_{\sigma \to 0_y} = constant = E_E \qquad (11)$$

$$\left.\frac{d\sigma}{d\varepsilon}\right|_{\sigma \to \sigma_y} = constant = E_E + E_C \qquad (12)$$

$$\sigma|_{phase\ 1} = \frac{1}{(K + \frac{A}{B})}\varepsilon \qquad (13)$$

$$\sigma|_{phase\ 3} = \left(\frac{1}{K}\right)\varepsilon - \frac{A}{K} \qquad (14)$$

From the model, phase 1 represents the incorporation of elastin only, phase 2 represents the onset of collagen recruitment, and phase 3 represent the complete recruitment of all collagen fibers. The mathematical equations provided model the stress-strain behavior where K, A, and B are model parameters. In this study, the main focus was on parameter A. Raghaven et al. calculated the value of parameter A for every donor whose age was known [5]. In our study, the value of parameter A was used to introduce the concept of critical strain, and help relate age to collagen content in the tissue.

Finite Element Method Modeling Approach

Abaqus 6.14 CAE/CFD computer modeling software was used to construct the structural geometry of a healthy abdominal aorta and an aneurysmal abdominal aorta of the aneurysm, to model the deformation as a function of time on healthy and aneurysmal aortas using the elastic modulus calculated from the data collected.

Tissue Property in FEM Model

The healthy aortic tissue properties typically display non-linear, anisotropic hyper-elastic or visco-elastic behavior. In this study, the analysis was conducted with the following assumptions: isotropic, non-linear, elastic modulus of 2.1 MPa, Poisson's ratio of 0.45, and arterial wall density of approximately 1200 Kg/m^3.

Geometry Construction in FEM Model

The structural geometry of healthy abdominal aorta resembles that of a pipe with a circular cross section of outer radius R and inner radius r, wall thickness w, and Length L. The geometry of a healthy abdominal aorta was constructed in ABAQUS with dimensions that are equivalent to the actual dimensions of the abdominal aorta. The outer radius of the abdominal aorta is approximately 1.5 cm, the wall thickness is approximately 2 mm, and the length ranges from 10 to 15 cm. For the aneurysmal aortic model, the same geometry configuration was constructed. A refined mesh was applied to the geometry which created at least 20,000 solid elements. The boundary conditions at the edge or end of the geometry may affect the mesh and may cause irregular deformation behavior in the model near the ends, thus the actual length of the geometry of the abdominal aortic model was extended by at least 2 cm on each end in order to account for this abnormal behavior.

Varying Tissue Properties in FEM Model

The aorta contains two major proteins, elastin and collagen. While elastin gives the ability to recoil, collagen provides the wall strength and holds smooth muscle tissues together. When the elastin or collagen in the aortic tissue start to degrade, the tissue will experience change in properties. To be able to study how growth takes place and be able to predict the rupture site, it was important to observe how the properties of the aortic wall change as growth occurs over time. One of the main properties of the tissue that will change with growth is the elastic modulus. In this analysis, the elastic modulus value calculated from the collagen degraded aortic specimen data was assigned to the aneurysmal section of the aortic model. A Stress-strain relationship analysis was observed based on the value of the elastic modulus.

Varying Non-Tissue Properties in FEM Model

In addition to varying tissue properties, external factors such as blood pressure must be considered. Many patients who suffer from hypertension also develop AAA at some point in their lives. Hypertension creates more force per unit area on the weak aneurysmal wall of the aorta causing an increase in diameter of the aneurysm and as a result an increased risk of rupture. In this study, systolic and diastolic blood pressure values were used in the analysis with lowest being the normal blood pressure value of 80 mmHg (or approximately 12000 N/m^2) and the highest being 120 mmHg (or approximately 16000 N/m^2).

Chapter 5

Data and Results

The experimental and finite element analysis results from this study are presented in this section and are discussed in-depth in the next section. The stress-strain data were plotted to show the uniaxial relationship between stress and strain for healthy longitudinal and circumferential AAA specimens and collagen degraded specimens, as shown in figures 34-37:

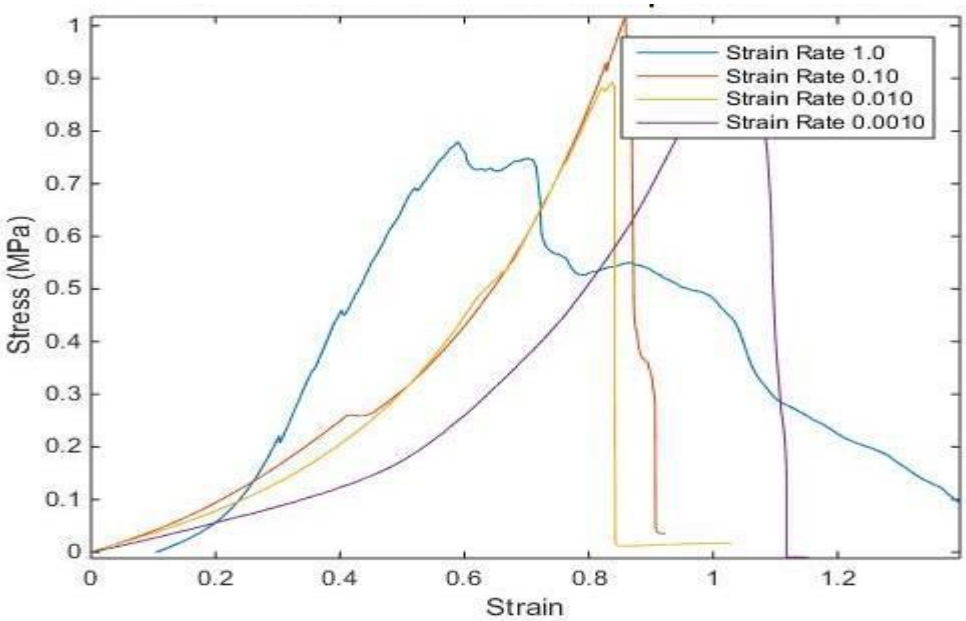

Figure 34 stress-strain relationship of healthy aortic tissue in the circumferential orientation at 4 different strain rates

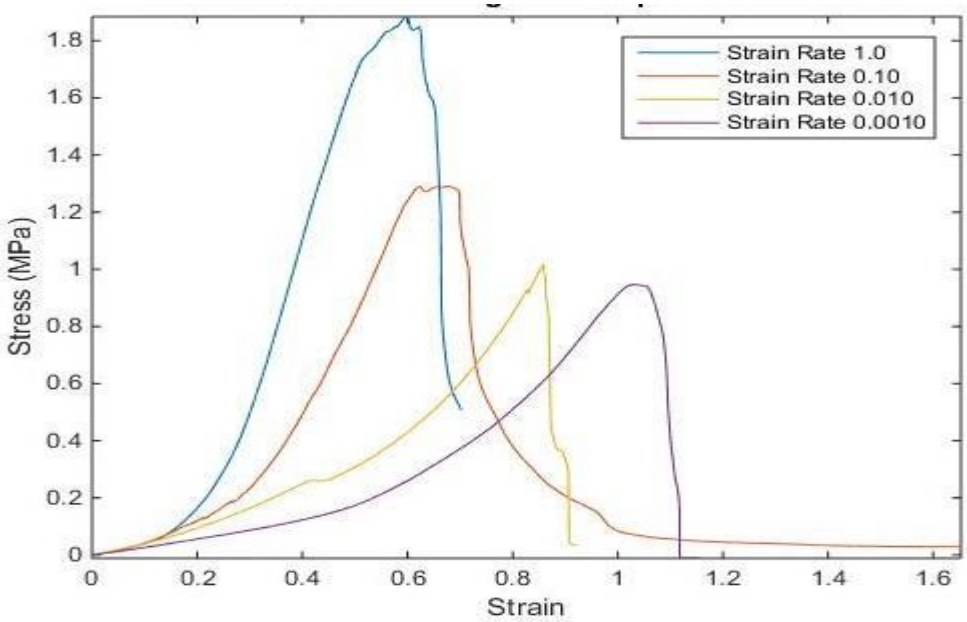

Figure 35 stress-strain relationship of healthy aortic tissue in the longitudinal orientation at 4 different strain rates

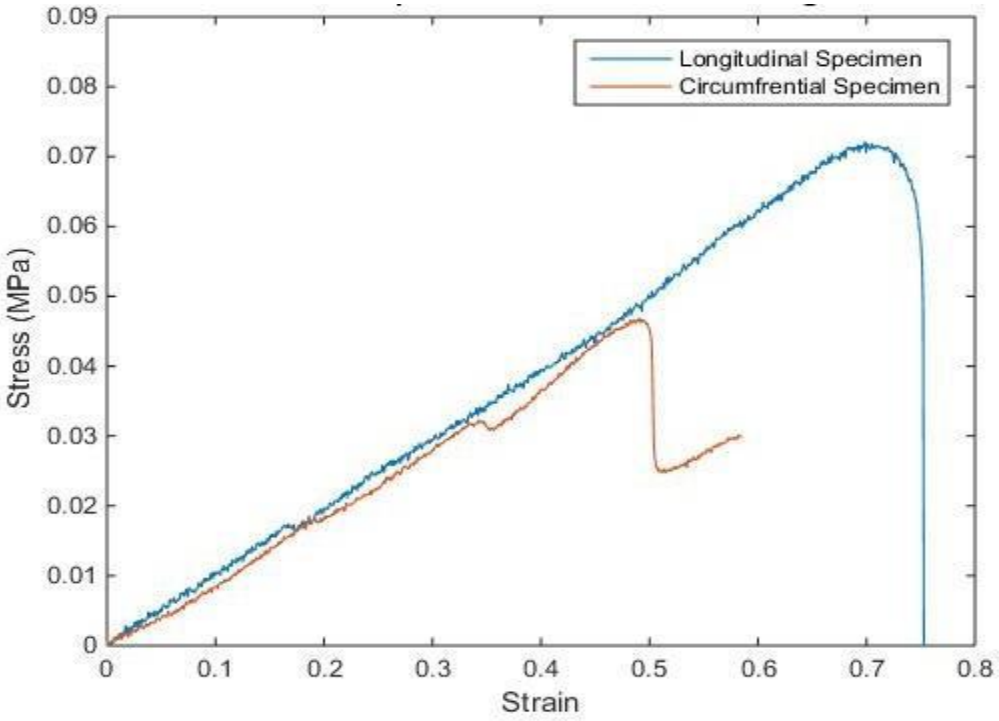

Figure 36 Stress-strain relationship of Collagen-degraded aortic specimens. Longitudinal orientation (blue line) and Circumferential Orientation (red line). The stress-strain relationship in the graph indicates that all the collagen was degraded and only elastin is present.

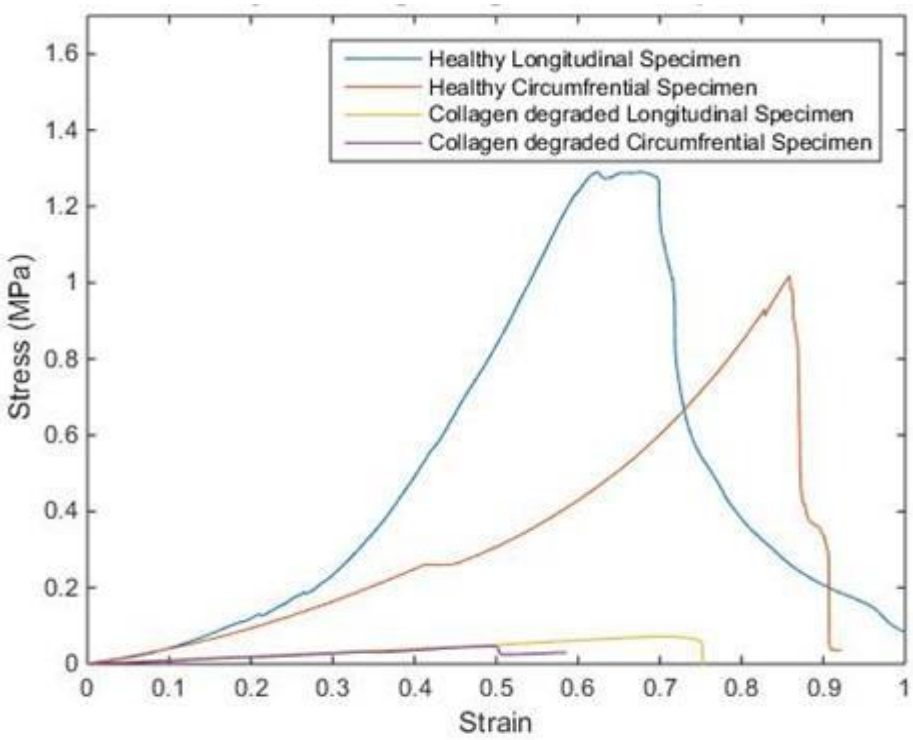

Figure 37 the stress-strain relationship for healthy and collagen-degraded specimens at strain rate of 1 mm/mm/min

Regression of the uniaxial testing data collected was performed in MATLAB. The data obtained from the uniaxial testing of longitudinal, circumferential, and collagen degraded specimens were fitted using MATLAB fitting toolbox. The root mean square errors of the best-fit did not exceed 7.2%. The fitted graphs are shown in figures 38-42:

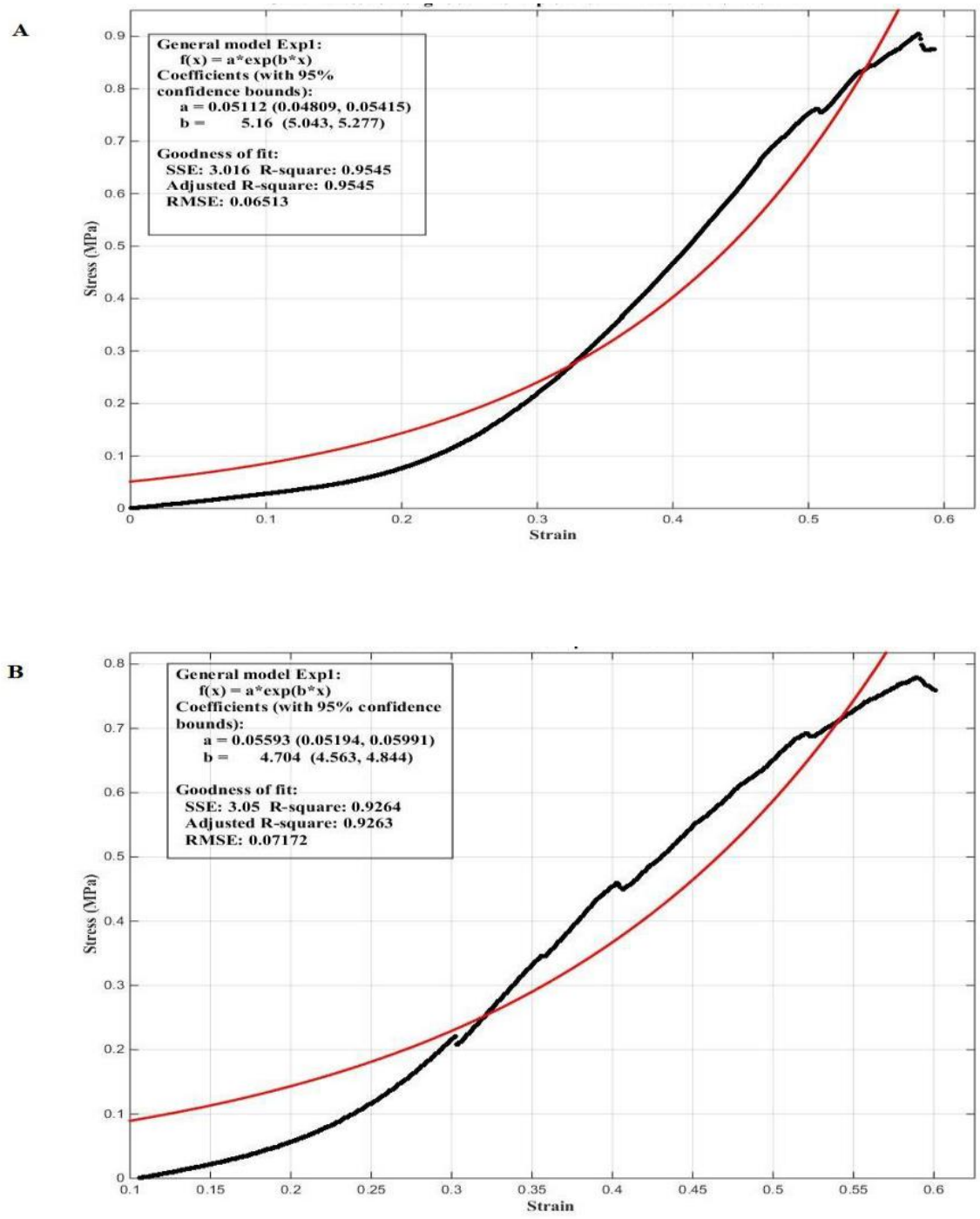

Figure 38 exponential fit of stress-strain data of longitudinal (A) and circumferential (B) healthy specimens at a strain rate of 1 mm/mm/min.

A

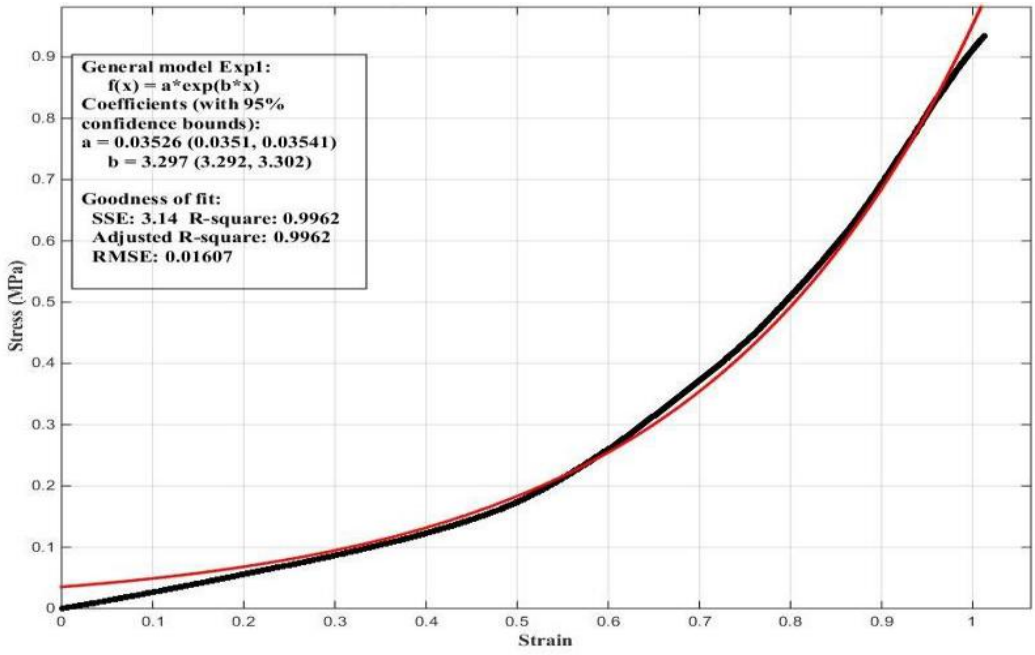

B

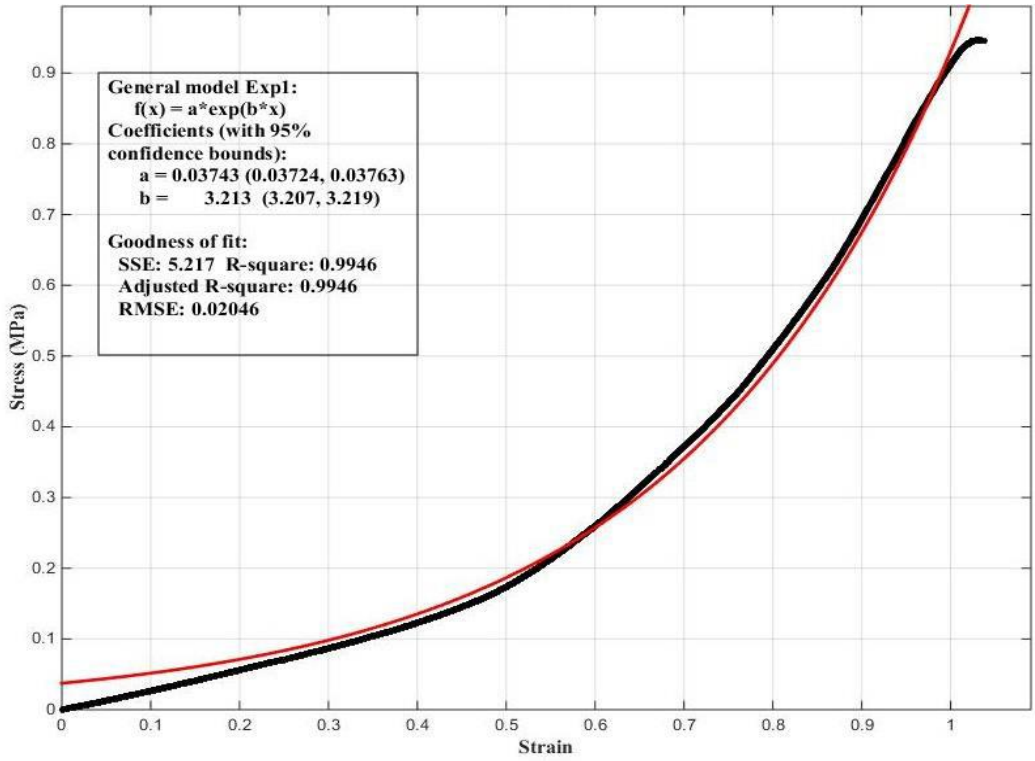

Figure 39 exponential fit of stress-strain data of longitudinal (A) and circumferential (B) healthy specimens at a strain rate of 0.1 mm/mm/min.

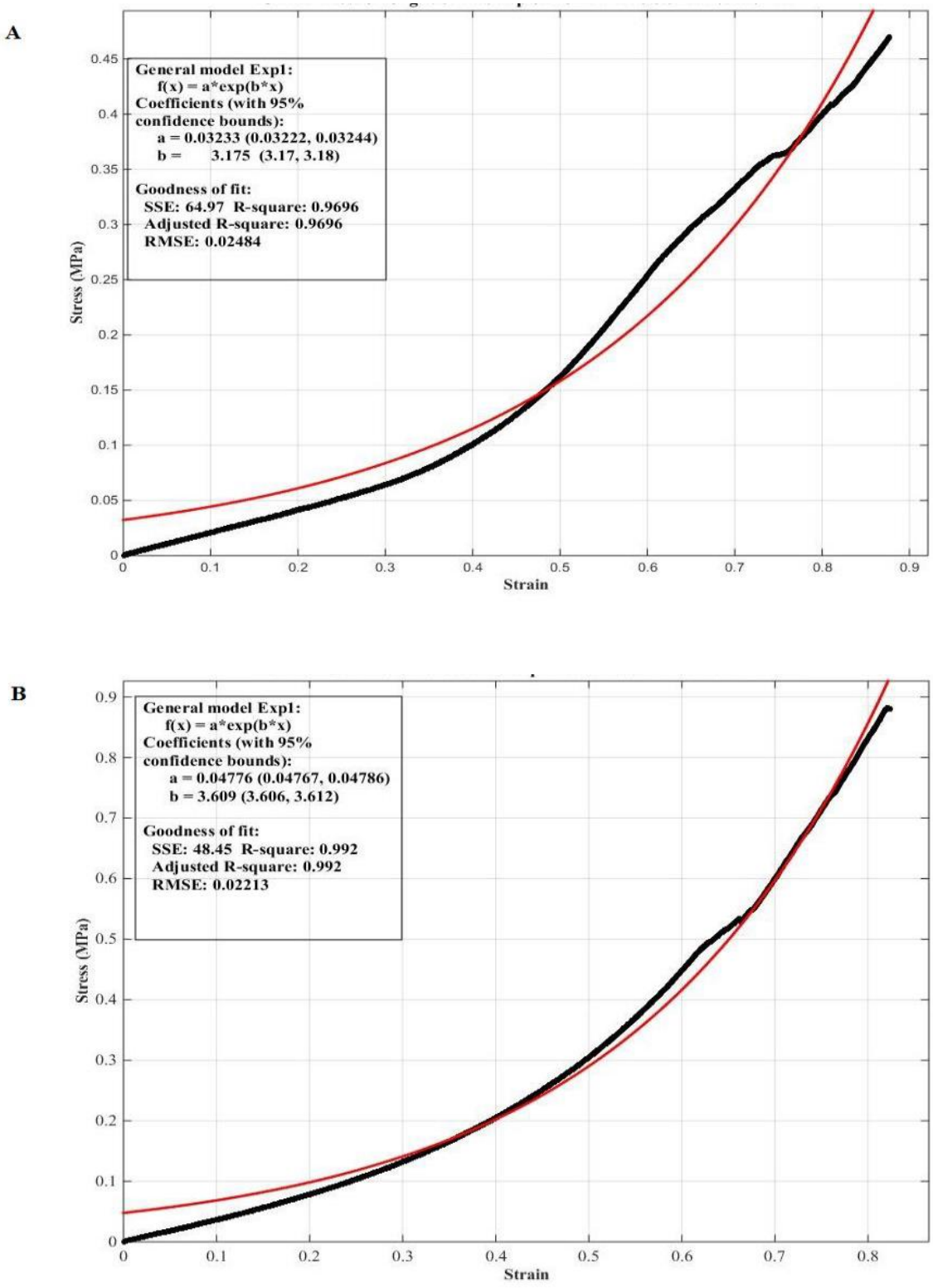

Figure 40 exponential fit of stress-strain data of longitudinal (A) and circumferential (B) healthy specimens at a strain rate of 0.01 mm/mm/min.

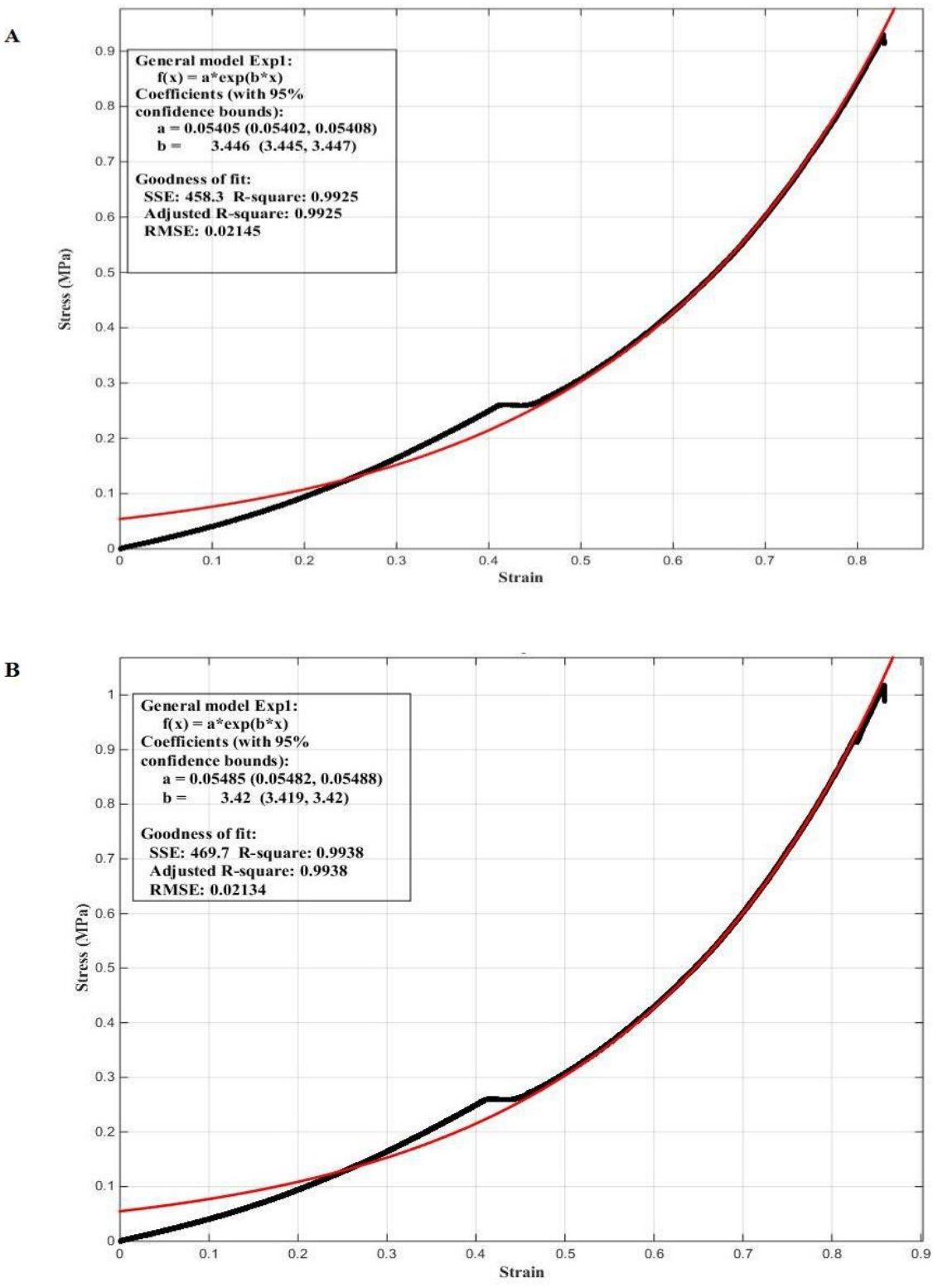

Figure 41 exponential fit of stress-strain data of longitudinal (A) and circumferential (B) healthy specimens at a strain rate of 0.001 mm/mm/min.

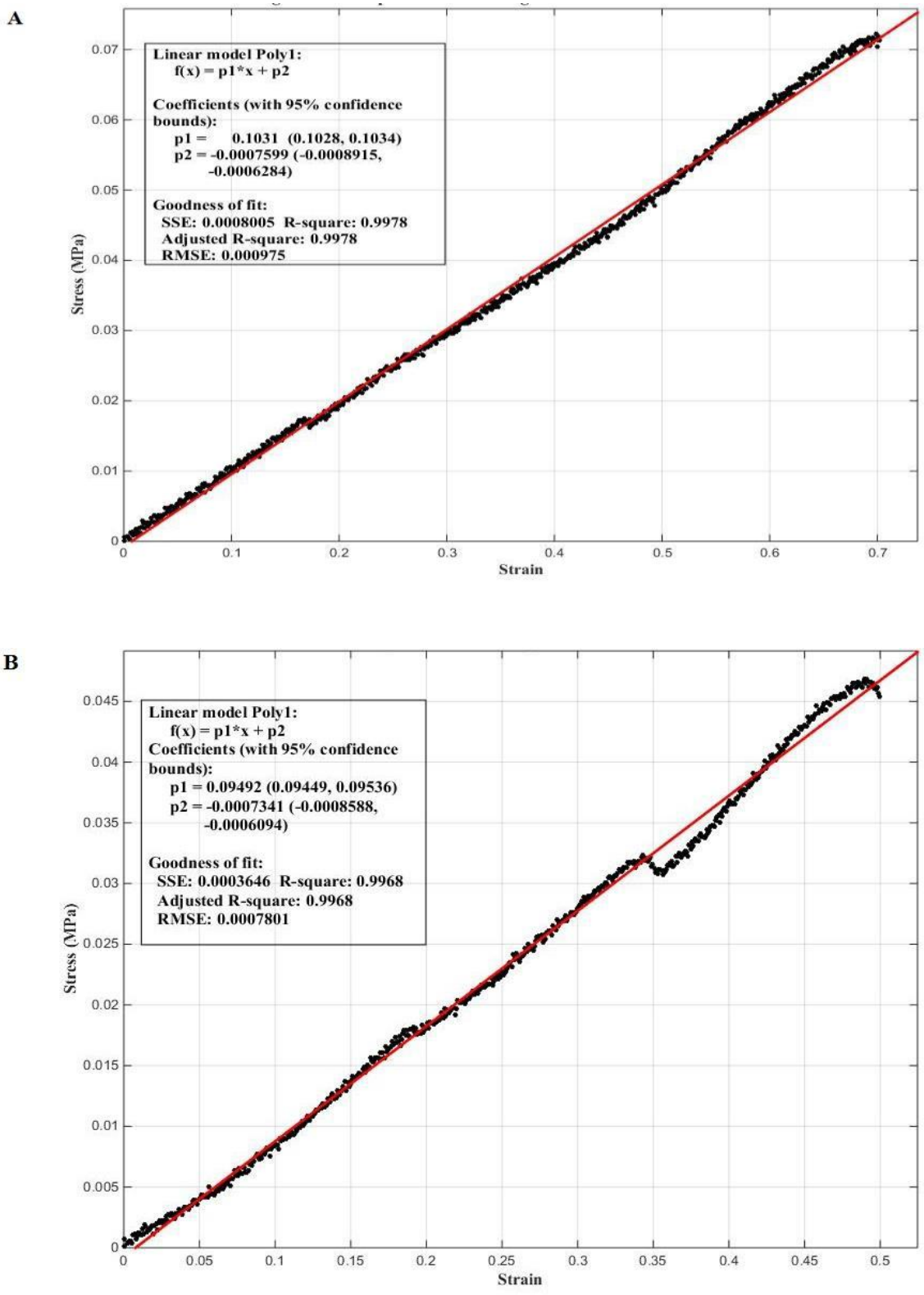

Figure 42 linear fit of stress-strain data of longitudinal (A) and circumferential (B) collagen-degraded specimen at a strain rate of 1 mm/mm/min.

A healthy abdominal aorta was modeled in ABAQUS. A cylindrical geometry was used with the following dimensions: Length of 14 cm, outside diameter of 3 cm, and thickness of 0.2 cm. The model was assigned an isotropic material behavior, elastic modulus value calculated from the experimental data, and a Poison's ratio of 0.45. The geometry was meshed using C3D8 8-noded hex elements type and has a total of 20,000 elements, as shown in figure 43. Pinned boundary condition was applied to each end.

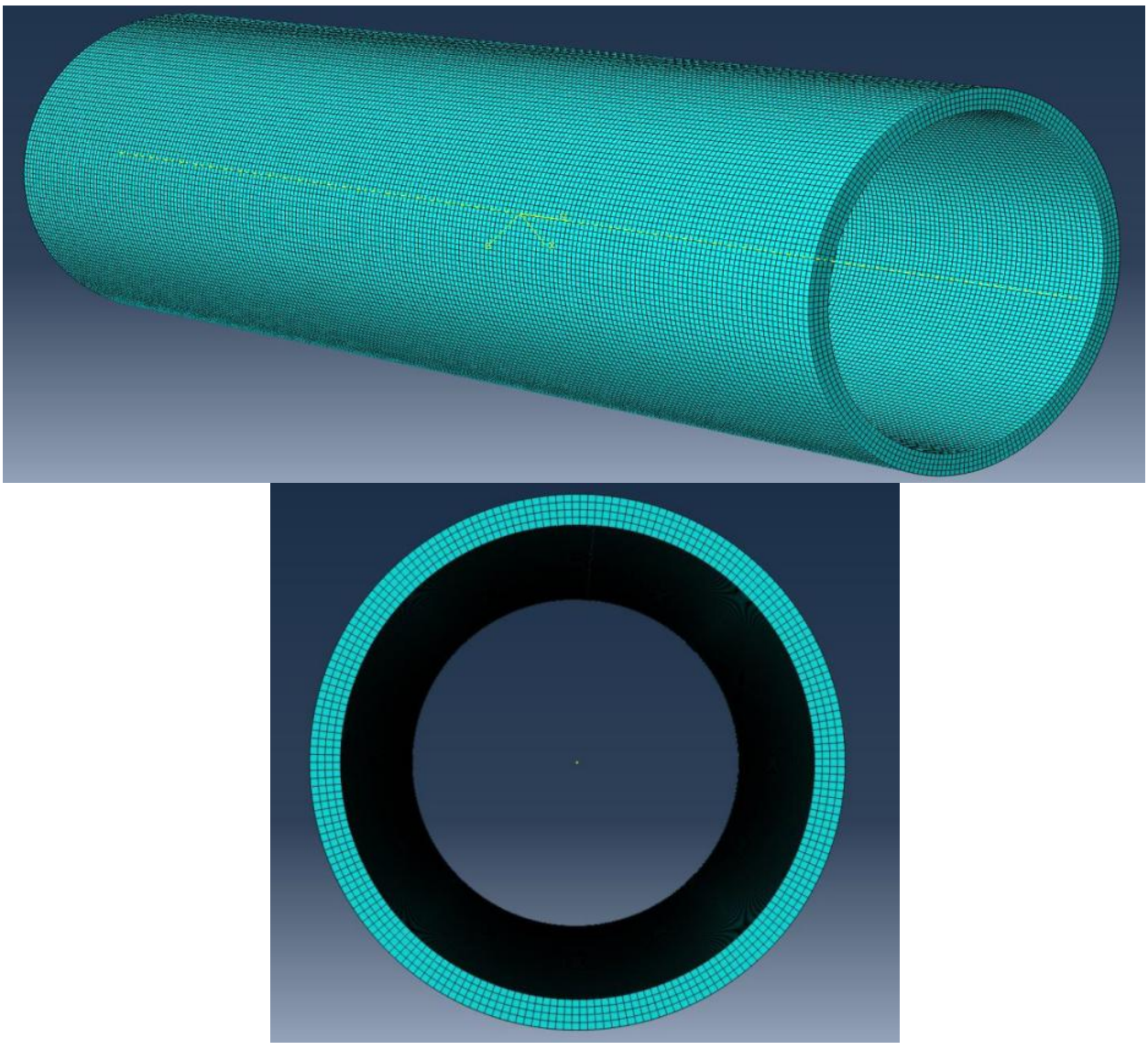

Figure 43 Constructed geometry of the aorta in ABAQUS.

An internal cyclic load of constant amplitude with a sinusoidal waveform, figure 44, was applied to the internal surface of the healthy aortic model.

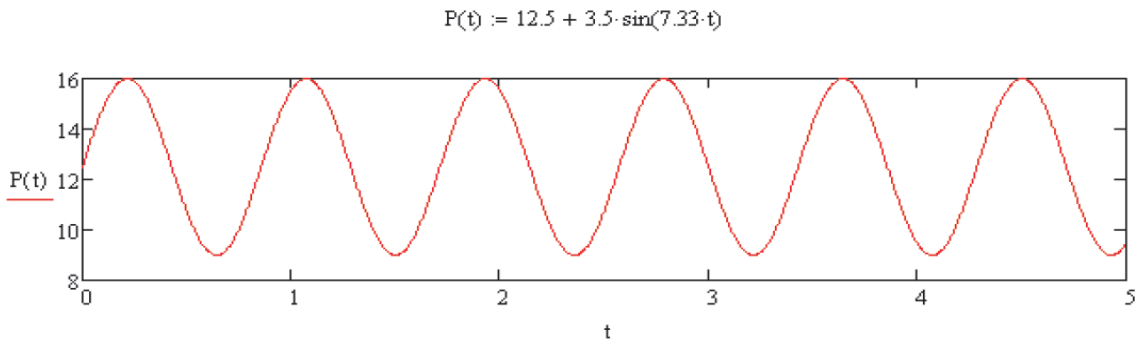

Figure 44 the sinusoidal function of blood pressure, the Y-axis is in units of kPa and the x-axis is in units of seconds [14].

The periodicity of the cyclic load was 10 seconds, and the resulting Von Mises stress distributions (kPa) were calculated upon applying the load and are shown in figure 45:

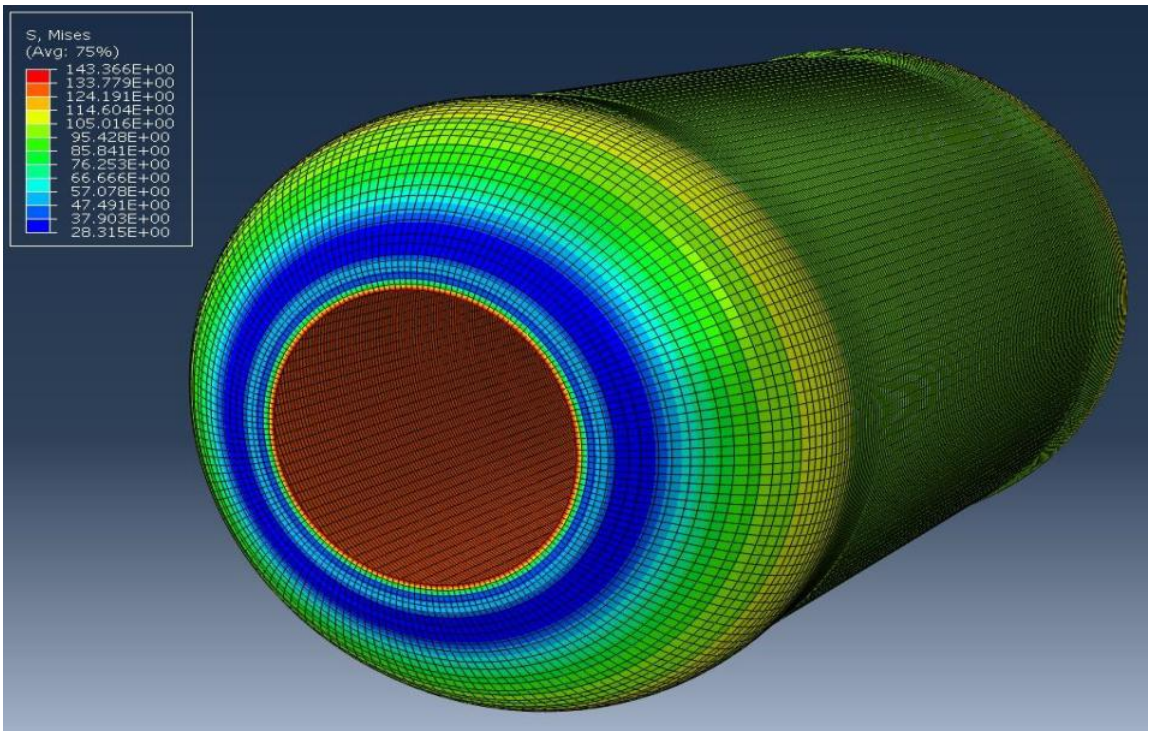

Figure 45 blood pressure values (stress distribution) during systole on the interior elements of the aorta

After completion of the Finite element analysis, one element was chosen from the healthy aortic tube model to illustrate the stress and circumferential strain magnitudes as a function of time (figure 46):

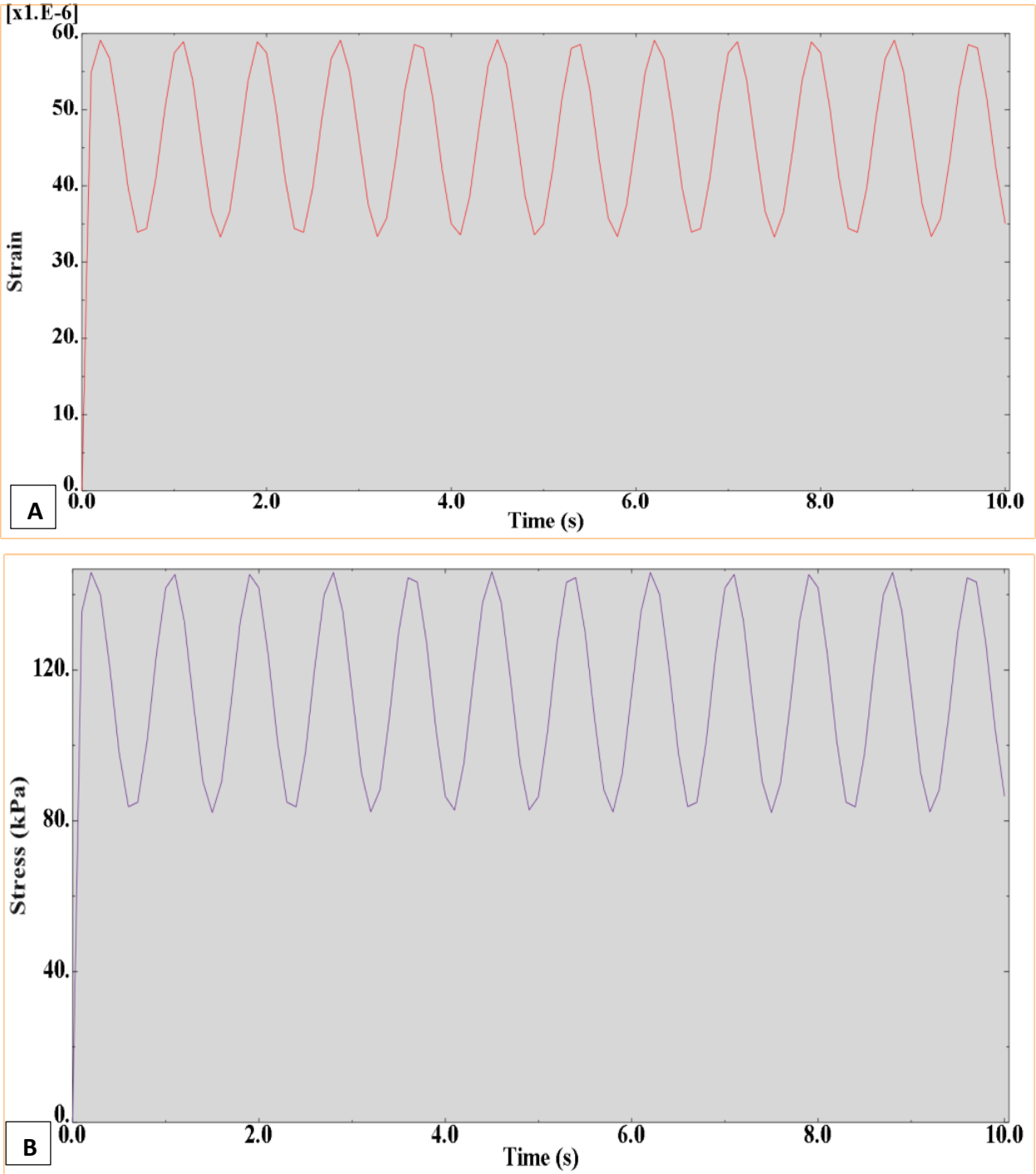

Figure 46 Max Principal strain (A) and Max Principal Stress (kPa) (B) over the time step interval for one element chosen from the interior of the healthy aortic model

An aneurysmal aortic model was implemented, too. For the aneurysmal model, the geometry and dimensions were the same as the healthy model. However, in the aneurysmal model, the tube was partitioned into 2 sections. One section was assigned the elastic modulus value of a healthy aortic tissue, and the second section was assigned the elastic modulus value of the collagen degraded aortic tissue, as shown below:

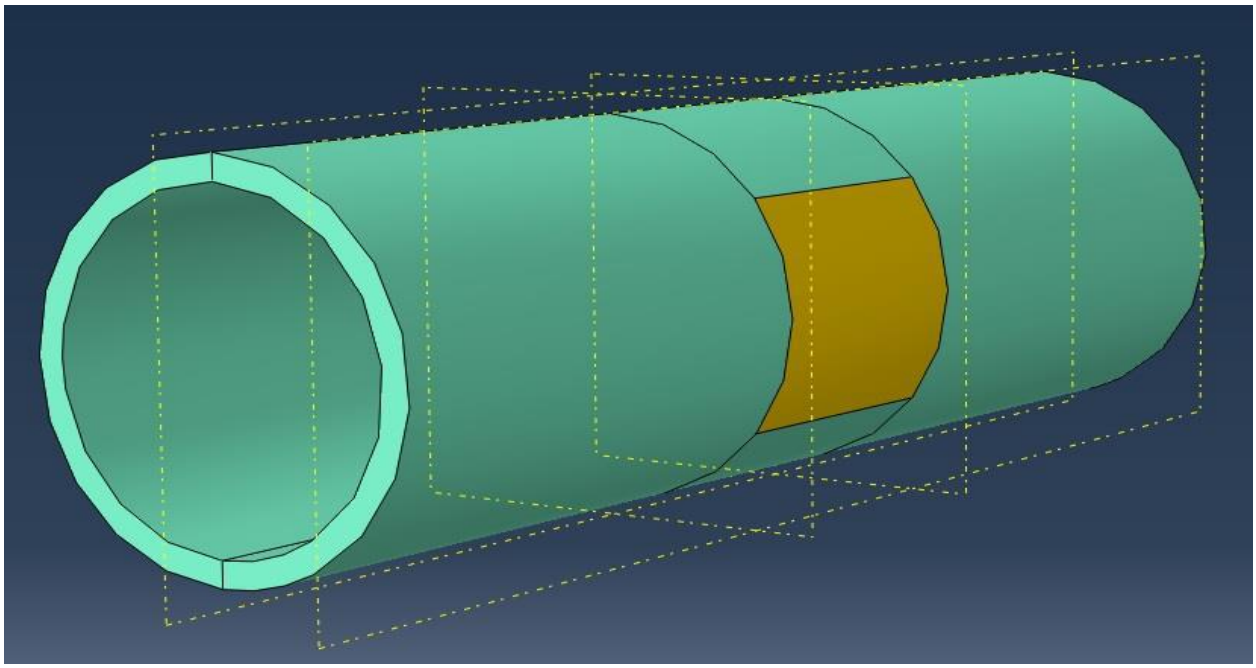

Figure 47 The green section is assigned the average elastic modulus value for the healthy aortic tissue. The yellow section is assigned the average elastic modulus value for collagen-degraded tissue.

The periodic load was applied over a step time of 10 seconds, and the resulting Von Mises stress distributions (kPa) were calculated upon applying the load and are shown in figure 48.

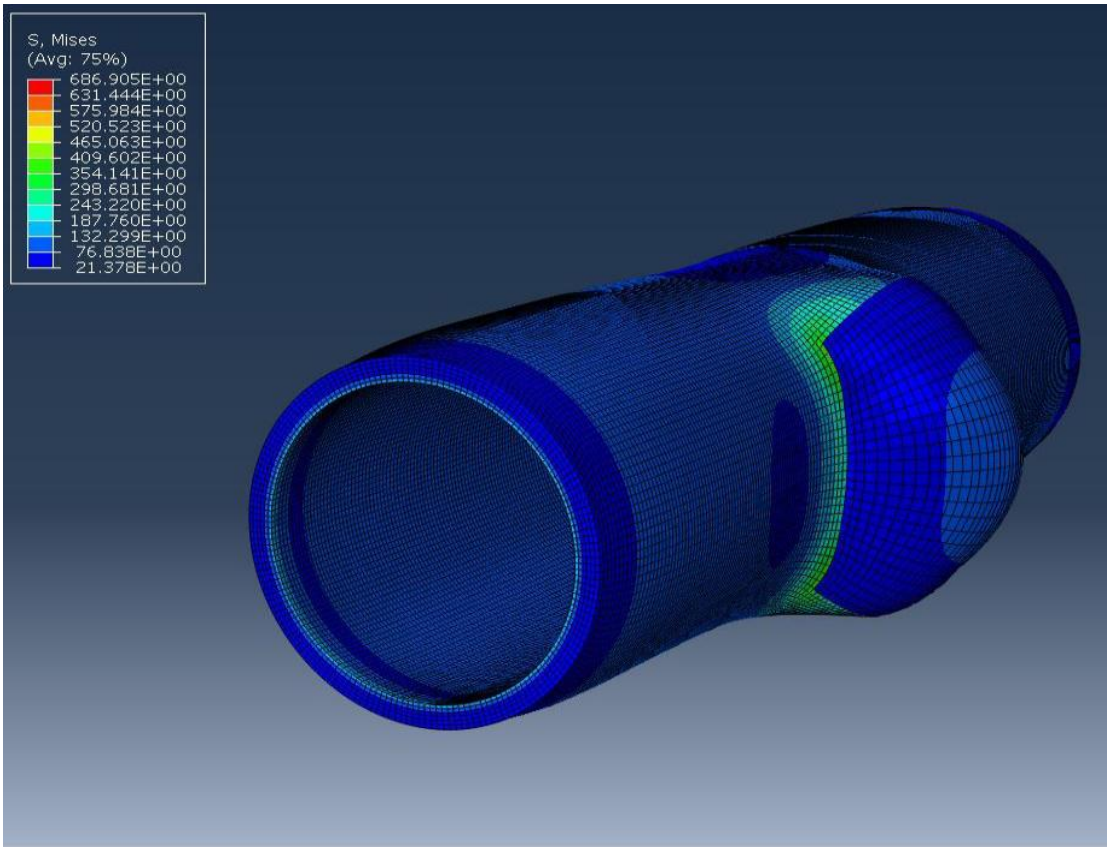

Figure 48 Von Mises stress values on the interior of the aneurysmal aortic model during diastole

After completion of the Finite element analysis, one element was chosen from the aneurysmal section of the aortic tube model to illustrate the stress and circumferential strain magnitudes as a function of time (figure 49):

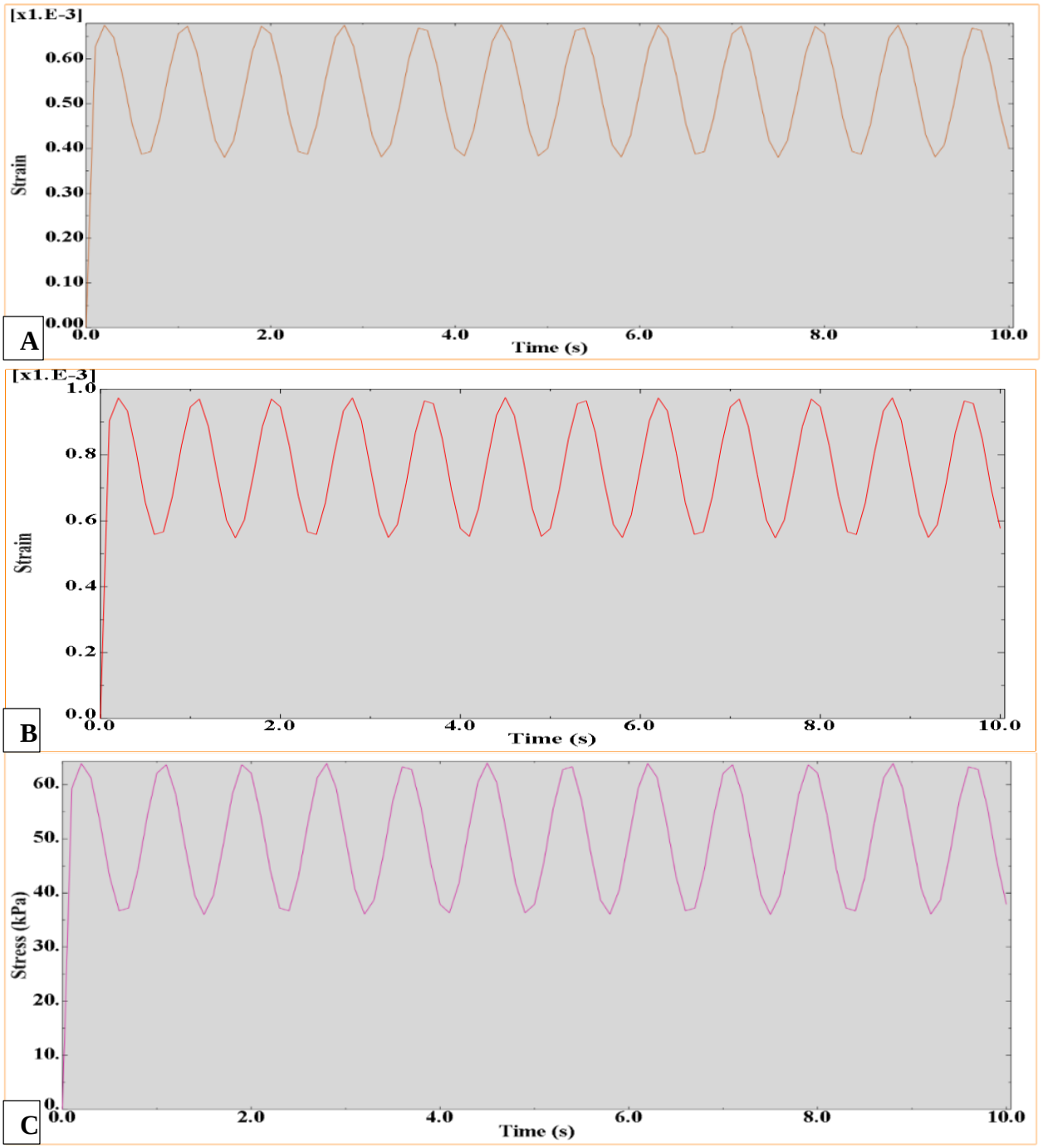

Figure 49 Radial strain (A), Circumferential Strain (B), and Max Principal Stress (C) over the time step interval for one element chosen from the interior of the aneurysmal aortic model.

Chapter 6

Discussion

In this study, the mathematical model developed by Raghaven et al. was used to describe the ex vivo biomechanical behavior of healthy and collagen degraded abdominal aortic specimens [5]. From the model, most attention was given to parameter A, which is defined as the point at which collagen fibers are fully engaged in the tissue due to the applied tension [5]. In this study, a more precise definition of parameter A is assigned where parameter A is also defined as the critical strain value (ε_c) that is related to expected strain at rupture. When the applied strain exceeds the critical strain value of the tissue, the tissue will be at a higher risk of rupture.

According to Raghaven biomechanics notes [13], the behavior of elastin and collagen is shown in figure 43:

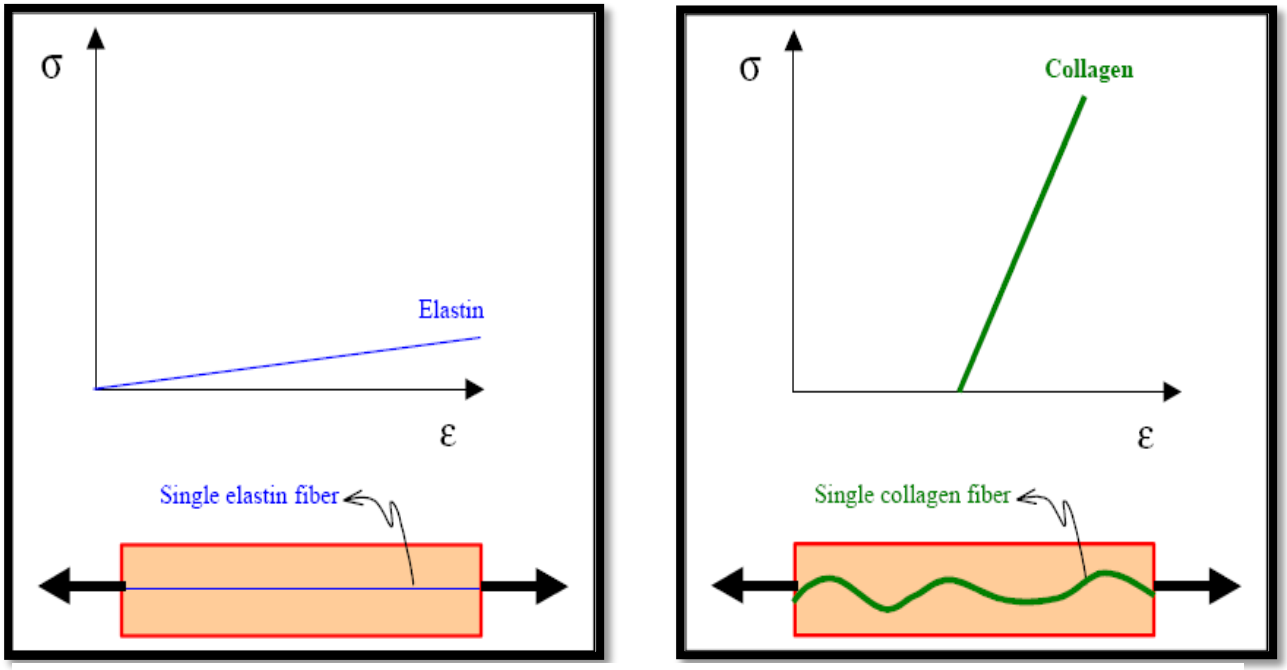

Figure 50 stress-strain relationship of elastin only (on left) and collagen only (on right) [13].

Initially, collagen fibers are loose and support minimal stress but they begin to uncoil after a certain strain point is reached. Elastin and collagen behavior by themselves are both linear

with vastly different elastic properties. However, when multiple strands of both types of fibers are in action, the resulting behavior appears to be exponential as shown in figure 44.

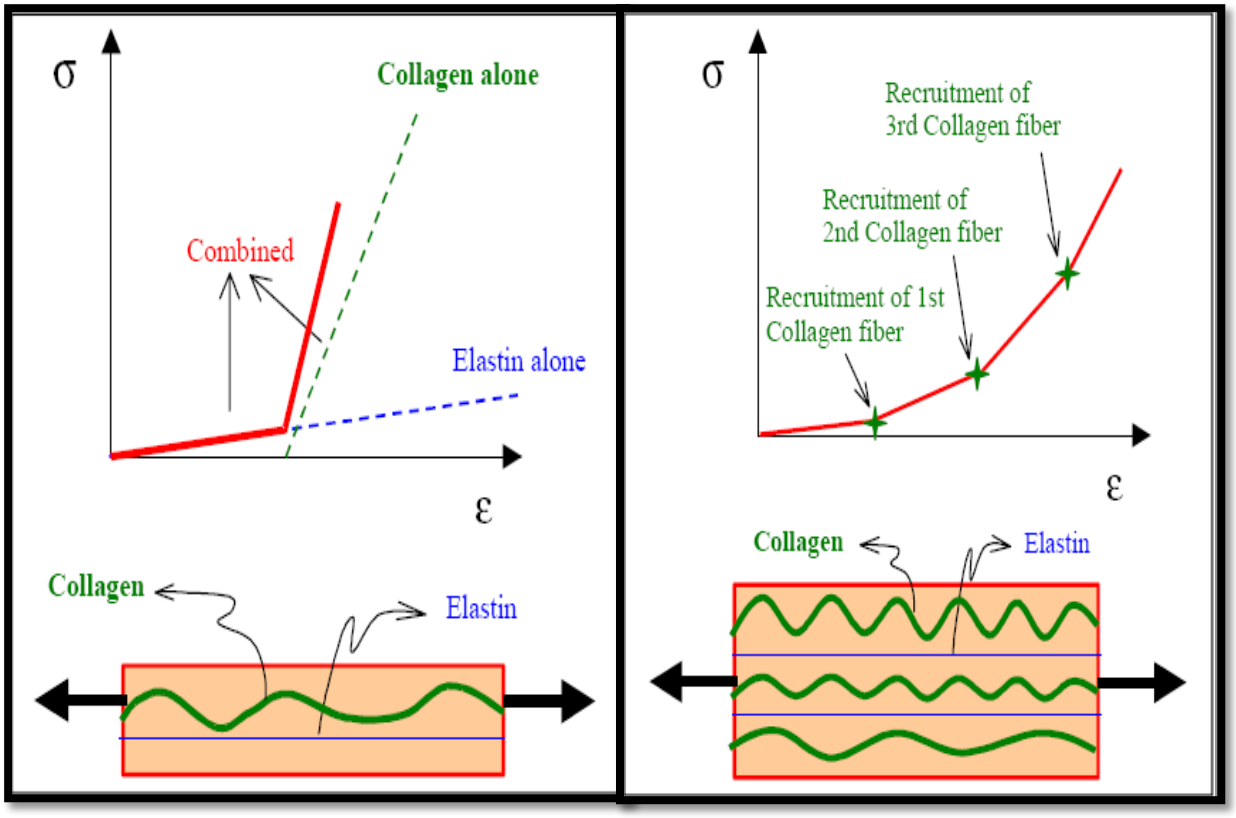

Figure 51 the combined stress-strain relationship of elastin and collagen [13].

The recruitment phases described previously in figure 33 are depicted schematically in the graph above where phase 1 represents the recruitment of the 1st collagen fiber, phase 2 represents the recruitment of the 2nd collagen fiber, and phase 3 represents the recruitment of all collagen fibers. Based on our study, when all collagen fibers are recruited, then the tissue is said to be at critical strain condition.

When collagen and elastin are both present in a healthy tissue, the tissue response to uniaxial tension will exhibit exponential behavior as shown previously in figures 34-35 from healthy specimens. Also, the uniaxial testing was performed at 4 different strain rates in order to

show how the average elastic modulus decreases for slower strain rates. On the other hand, looking at collagen degraded uniaxial test results in figure 36, the specimens exhibit a linear behavior under uniaxial tension. This behavior resembles the behavior suggested by Raghaven studies [5][13]. Thus, it supports the notion that collagen did degrade, and elastin is the only component of the tissue material available in the tissue to support the load.

Collagen is important for the tissue to maintain its strength. If only elastin fibers are present, the tissue will be much weaker. As a result, the tissue will have a very low critical strain value. Consequently, the tissue will be at a much higher risk of rupture.

Many studies assess the biomechanical behavior of human AAA and rupture risk in vivo using modern imaging techniques, geometry reconstruction software, and finite element analysis software. However, it is not sufficient to rely solely on imaging. It is essential to observe actual tissue biomechanics through ex vivo mechanical testing. This study focuses on evaluating tissue properties using ex vivo mechanical testing and using those properties in the finite element models in ABAQUS. As a result, AAA growth kinetics and rupture risk assessment will be more accurate.

When comparing the average elastic modulus for healthy tissue with the average elastic modulus for collagen degraded tissue, it is noticeable that the collagen degraded tissue is less compliant or stiffer than the healthy tissue. The decrease in stiffness can be due to collagen degradation in the tissue which leads to smooth muscle degradation [3][12]. Such change in tissue properties alters the biomechanical behavior of the tissue as shown previously in the collagen degraded stress-strain relationship in figure 36.

The value of parameter A was calculated for and associated with each AAA specimen donor in Raghaven et al. study [5]. Table 3 shows the calculated values of parameter A for aneurysmal donors and their corresponding age group. As stated in chapter 3, equation 14 was used by Raghaven to calculate A.

$$\sigma_{phase\ 3} = \left(\frac{1}{K}\right)\varepsilon - \frac{A}{K} \qquad (14)$$

Table 3 Parameter A calculated values for donors with the ages listed from Raghaven et al. study [5].

DONOR	AGE	A	A CORRECTED
1	47	0.132	0.116
2	31	0.294	0.231
3	34	0.193	0.155
4	60	0.088	0.084
5	48	0.126	0.111
6	58	0.429	0.403
7	49	0.298	0.265

In order to have a better assessment of collagen degradation due to aging, our study focused on comparing our results with Raghaven et al. results [5]. For healthy AA specimens and collagen degraded specimens, the average E values, parameter A (critical ε), average maximum stress, and average maximum strain (ε at rupture) are shown in Table 4.

Table 4 calculated values of average elastic modulus, parameter A, average uniaxial max stress, and average max strain for all the specimens used in the study.

Specimens Group	Average E (MPa)	A (ε_c)	Average max σ (MPa)	Average max ε (ε at rupture)
Healthy longitudinal (N=12)	1.8981 ± 0.4296	0.3869 ± 0.0556	0.8126 ± 0.1133	0.8598 ± 0.1178
Healthy circumferential (N=12)	2.3505 ± 0.1811	0.4391 ± 0.0754	0.9344 ± 0.0678	0.8743 ± 0.1248
Collagen degraded longitudinal (N=6)	0.1031 ± 0.0073	0.0074 ± 0.0003	0.0734 ± 0.0013	0.6827 ± 0.1522
Collagen degraded circumferential (N=6)	0.0949 ± 0.0042	0.0077 ± 0.0002	0.0468 ± 0.0021	0.4904 ± 0.1034
Values given as	Mean ± SEM			

When comparing the values of parameter A calculated in our study (Table 4) with the values of parameter A in Raghaven et al. study (Table 3), we conclude that the higher value of A for a healthy tissue with normal collagen content is an indicative of an age younger than 30 years old. However, in Raghaven et al. study [5], the A value for donors 6 and 7 are higher than the A values for donors 2 and 3. Such discrepancy could be an artifact of how the value of A was calculated in their study. This deserves a more in depth analysis that reassess the physical significance of parameter A, as observed in our study where the A values for all of our specimens were calculated. It is shown in Table 4 that the A values are smaller for collagen degraded specimens than for healthy specimens. As collagen degrades in the tissue, the A value (ε_c) decreases. Consequently, the tissue weakens and will not be able to withstand moderate to

high stress. In addition, our study indicates that collagen degrades as humans' become older based on associating parameter A (critical strain ε_c) values with the corresponding age of each donor from Raghaven et al. study [5]. Thus, the risk for rupture also increases severely with age. The equation adapted from Raghaven et al. study can be rewritten as:

$$\sigma_{phase\ 3} = \left(\frac{1}{K}\right)\varepsilon - \frac{\varepsilon_c}{K} \qquad (15)$$

From the results of the Finite Element Analysis for an axisymmetric healthy tube, the stress is constant along the length and circumference of the cylinder due to the isotropic material property assigned. Also, the maximum values of pressure are on the internal surface of the tube. The axisymmetric bulging of the healthy tube in figure 45 resembles the bulging behavior of a healthy abdominal aorta in humans.

When comparing the healthy tube stress values with the aneurysmal tube stress values in figures 45 and 48, respectively, it can be seen that the tube was bulging more in section 2 (the collagen degraded section, yellow) at lower values of pressure. This observation proves the importance of collagen in maintaining tissue strength and the ability to resist high strain values at higher pressures. Thus, it can be concluded that hypertension patients who develop abdominal aortic aneurysms need to monitor the growth of the aneurysmal more often than patients who do not have blood pressure problems.

In addition, when comparing the max principal strain values for one element in the healthy tube with one element from the aneurysmal section in the aneurysmal tube in figures 46 and 49, respectively, it can be seen that the max strain for the aneurysmal element has increased by approximately a factor of 10 times that of the healthy element. Thus, collagen presence in the tissue plays a vital role in maintaining the necessary support needed for resisting strain and withstanding high stresses.

The blood pressure assigned in the analysis was approximately in the range of 80 mmHg to 145 mmHg. No hypertension blood pressure values were assigned, because the focus needed to be on one variable (collagen content in the tissue). Focusing on such variable will allow us to have better and accurate prediction of rupture criteria for a specific group of patients who suffer from collagen degradation due to genetics or age.

Many causes contribute to developing AAA such as smoking, hypertension, gender, and genetics. Realistically, the pathogenesis of AAA is not only dependent on the biomechanics, rather it is a combination of biomechanics, genetics, and external causes or behavior. However, the biomechanics portion of the pathogenesis must be considered because it accounts for a big portion of the problem. Thus, analyzing the biomechanical behavior as far as stress-strain relationships and fluid-structure interactions will contribute significantly to answering many questions regarding the development and growth of AAA, and it will help in contributing to the overall solution of the pathogenesis.

Observing the stress-strain relationships in aneurysms helps in evaluating the patient's case. It is important to be able to predict the stage of the diseased aneurysm and approximate the amount of time left until rupture occurs. Stress-stain relationships allows for such a prediction to take place because it can determine the site that is under the highest stress or strain. However, the computations made by FEM software may not be accurate if the input parameters do not accurately resemble those of the aneurysmal tissue properties. Thus, it is important to improve upon experimental data in order to better improve the modeling aspect of the problem, which will ultimately lead to a more precise prediction of rupture site and remaining time until rupture.

Under physiological conditions, the stress applied on the aorta is not uniaxial, rather, it is biaxial. Relying on uniaxial testing is not sufficient, and studying the stress-strain behavior of

aortic tissue under biaxial stress is needed. Conducting biaxial testing on artic specimens will help us validate the accuracy of critical strain values that were calculated in this study as rupture criteria parameters. Also, biaxial tension tests will allow us to obtain constants that relate to the property of orthotropic and anisotropic materials. Ultimately such constants will be input into FEA software such as ABAQUS in order to create a more accurate finite element models and analysis of AAA, and, more importantly, to develop a more accurate risk assessment values.

In addition, other factors that potentially affect AAA growth are blood pressure and blood flow, as mentioned previously. Altering pressure values will impact the velocity of the blood flowing through the aorta due to the increase in heart rate. Thus, Laminar vs. Turbulent flow behavior will take place in the aneurysmal aorta. It is very important to study the fluid-structure flow of turbulent behavior, because turbulent fluid-flow of blood causes the formation of intraluminal thrombus on the aneurysm wall. Once a thrombus mass is formed on the aneurysmal wall, the turbulence in the blood flowing through the aneurysm will pick up small emboli from the thrombus mass. Blood will carry the small emboli to the arterioles and venules which may cause blood clots and, eventually, strokes. Thus, it is important to observe turbulent flow and incorporate its presence in the risk analysis and in the prognostics to avoid catastrophic situations of rupture or strokes [8][9][10].

One other variable that will be affected, by the change in velocity and type of flow, is the shear stress on the inside wall of the aorta. Elevated shear stress will cause the intima layer of the aortic wall to degrade at a faster rate, which results in weakening of the aortic wall. Such analysis must be considered as we move on to develop more accurate rupture criteria. Shear stress changes when altering velocity of the fluid and, in turn, alters the flow-type of the blood [8].

Chapter 7

Conclusions

Over the past decade, significant new research in modeling AAA and predicting rupture site has been conducted, and advancements in technology have allowed many new techniques to be introduced that facilitate better assessment of potential for rupture in AAA patients. These techniques have made it possible to incorporate factors that are used to predict rupture in AAA such as gender, age, family history, smoking status, hypertension, aneurysm size, aneurysm diameter, and intraluminal thrombus thickness in the models in assessing the risk of rupture [1][3][8]. However, maximum diameter criteria still remains the main rupture assessment tool in order to decide if surgical intervention is needed.

This study is devoted to the development of new criteria to assess rupture risk of AAA. In fact, an accurate and reliable stress-strain analysis of an aneurysm is still needed. It will allow us to create not only a precise three-dimensional solid model but also assign more accurate material properties.

Our study elucidates the effect of collagen degradation in AAA rupture and how it can be used to select a more accurate rupture criteria. From a biological point of view, collagen degradation occurs due to the action of collagenases, which are a class of proteases enzymes. Some of the collagenases that are prevalent in growing and ruptured AAAs are neutrophil collagenase and cysteine collagenase K, L, and S [16]. Excessive collagenase activity causes weakening and destruction of the aortic wall. In fact, biomechanical studies have shown that collagen present in media and adventitia layers of the aortic wall is responsible for maintaining tissue microstructural stability [16]. This study shows how the biomechanical relationship of the aortic tissue changes due to the absence of collagen in the tissue. It is indicted that collagen degradation weakens the tissue and alters its microstructure. To our knowledge, this study is the

first to examine the biomechanical behavior of the aortic tissue after complete degradation of collagen.

From the results of this study, it is observed that an aneurysm causes significant changes in the biomechanical properties of the aortic tissue. The results indicate that changes in tissue's collagen microstructure, due to degradation, critical strain to rupture will be a better indicator for implementing rupture in AAA.

In the literature, the tissue property of the aorta is reported as being anisotropic. Our study shows that the elasticity of the longitudinal and circumferential orientation of the tissue is approximately the same, making it at least orthotropic. Thus, justifying our assumption of isotropic behavior in the ABAQUS model. Although assumptions such as isotropy can result in under estimation of strain and stress values, the results are still significant when compared to other models in the literature. To our knowledge, this is the first work to divide the aortic tube model into two sections, and assign each section an elastic modulus of healthy and collagen degraded tissues, respectively. It is shown that aneurysm forms in the tissue region where collagen degradation occurs, and potential rupture is more likely to occur in that region. In literature, AAA modeling is via conducting finite element analysis on constructed geometry from CT scans taken from AAA patients or constructed an aneurysm geometry and analyzed the stress., rather than observing the growth of AAA from an initial stage.

In future studies, the focus on obtaining more accurate data through intensive testing of abdominal aortic tissue can improve upon the current accuracy of the models. Performing biaxial testing on aneurysmal aortic tissue, modeling fluid-structure interaction in an aneurysm, and studying the effects of intraluminal thrombus on peak wall stress should be considered in evaluating rupture assessment of AAA [8][9] [10][15].

References

1. Doyle, Barry J. *3D Imaging of Abdominal Aortic Aneurysms Techniques and Applications*. Hauppauge, N.Y.: Nova Science, 2010.

2. Humphrey, J. D., & Taylor, C. A. (2008). Intracranial and Abdominal Aortic Aneurysms: Similarities, Differences, and Need for a New Class of Computational Models. *Annual Review Of Biomedical Engineering*, *10*(1), 221-246. doi:10.1146/annurev.bioeng.10.061807.160439

3. Vorp, D. A., & Vande Geest, J. P. (2005). Biomechanical determinants of abdominal aortic aneurysm rupture. *Arteriosclerosis, Thrombosis, And Vascular Biology*, *25*(8), 1558-1566.

4. Greenhalgh, R. M., Brown, L. C., & Powell, J. T. (2010). Endovascular Repair of Abdominal Aortic Aneurysm. *New England Journal Of Medicine*, *363*(15), 1479. doi:10.1056/NEJMc1007807

5. Raghavan, M. L., Webster, M. W., & Vorp, D. A. (1996). Ex vivo biomechanical behavior of abdominal aortic aneurysm: assessment using a new mathematical model. *Annals Of Biomedical Engineering*, *24*(5), 573-582.

6. Vande Geest, J. P., Di Martino, E. S., Bohra, A., Makaroun, M. S., & Vorp, D. A. (2006). A biomechanics-based rupture potential index for abdominal aortic aneurysm risk assessment: demonstrative application. *Annals Of The New York Academy Of Sciences*, *1085*11-21.

7. Gasser, T. C., Auer, M., Labruto, F., Swedenborg, J., & Roy, J. (2010). Biomechanical rupture risk assessment of abdominal aortic aneurysms: model complexity versus predictability of finite element simulations. *European Journal Of Vascular And Endovascular Surgery: The Official Journal Of The European Society For Vascular Surgery*, *40*(2), 176-185.

8. Biasetti, J., Spazzini, P. G., Swedenborg, J., & Christian Gasser, T. (2012). An integrated fluid-chemical model toward modeling the formation of intra-luminal thrombus in abdominal aortic aneurysms. *Frontiers In Physiology*, *3*1-16.

9. Mower, W. R., Quiñones, W. J., & Gambhir, S. S. (1997). Effect of intraluminal thrombus on abdominal aortic aneurysm wall stress. *Journal Of Vascular Surgery*, *26*(4), 602-608.

10. Zelaya, J. E., Goenezen, S., Dargon, P. T., Azarbal, A., & Rugonyi, S. (2014). Improving the efficiency of abdominal aortic aneurysm wall stress computations. *Plos One*, *9*(7), e101353.

11. Vorp, D. A., Raghavan, M. L., & Webster, M. W. (1998). Mechanical wall stress in abdominal aortic aneurysm: influence of diameter and asymmetry. *Journal Of Vascular Surgery*, *27*(4), 632-639.

12. Choke, E., Cockerill, G., Wilson, W. W., Sayed, S., Dawson, J., Loftus, I., & Thompson, M. M. (2005). A review of biological factors implicated in abdominal aortic aneurysm rupture. *European Journal Of Vascular And Endovascular Surgery: The Official Journal Of The European Society For Vascular Surgery*, *30*(3), 227-244.

13. Raghaven, M. (n.d.). Cardiovascular Bio-solid Mechanics Section. In *BIOMECHANICS 51:050* (pp. 3-25). Iowa: M. L. Raghaven.

14. Wilson, C. (2008). Abaqus Abdominal Aortic Aneurysm Model. In *NONLINEAR FINITE ELEMENT ANALYSIS OF AN ABDOMINAL AORTIC ANEURYSM*. UMI Microform.

15. Polzer, S., Gasser, T. C., Bursa, J., Staffa, R., Vlachovsky, R., Man, V., & Skacel, P. (2013). Importance of material model in wall stress prediction in abdominal aortic aneurysms. *Medical Engineering & Physics*, *35*(9), 1282-1289. doi:10.1016/j.medengphy.2013.01.008

16. Abdul-Hussien, H., Soekhoe, R. V., Weber, E., von der Thüsen, J. H., Kleemann, R., Mulder, A., & Lindeman, J. N. (2007). Collagen degradation in the abdominal aneurysm: a conspiracy of matrix metalloproteinase and cysteine collagenases. *The American Journal Of Pathology*, *170*(3), 809-817.

17. The Top 10 Causes of Death. (2012). Retrieved October 26, 2015, from http://www.who.int/mediacentre/factsheets/fs310/en/

18. Projections of the Population by Selected Age Groups and Sex for the United States: Table 2. 2015 to 2060 (NP2012-T2). Release Date: December 2012. Source: U.S. Census Bureau, Population Division at http://www.census.gov/population/projections/files/summary/NP2012-T2.xls.

19. Tsamis A, Krawiec JT, Vorp DA. 2013 Elastin and collagen fibre microstructure of the human aorta in ageing and disease: a review. J R Soc Interface 10:20121004. http://dx.doi.org/10.1098/rsif.2012.1004

20. Wilmink, T. B., Quick, C. R., & Day, N. E. (1999). The association between cigarette smoking and abdominal aortic aneurysms. *Journal Of Vascular Surgery*, *30*(6), 1099-1105.